Australian Government
Department of Defence
Defence Science and
Technology Organisation

Simple Detection-Performance Analysis of Multistatic Sonar for Anti-Submarine Warfare

M.P. Fewell and S. Ozols

Maritime Operations Division
Defence Science and Technology Organisation

DSTO-TR-2562

ABSTRACT

This report describes a method of deriving the detection performance of a multistatic sonar field from the performance of a field of similar sonars operated monostatically. It allows a direct comparison of the two modes of operation, thereby quantifying the advantage, if any, of multistatics. The method is derived from the sonar equation in the noise-limited regime. We also compare two different network architectures for tracking: each receiver performing its own tracking or detection information being passed to a central tracking node. We start with three schematic monostatic detection-probability curves, ranging from almost a cookie cutter to an exponential shape, which has a long low-probability tail. We find that networking, whether to perform multistatics or to centralise tracking, brings no advantage for a cookie-cutter detection probability. With the exponential shape, on the other hand, a multistatic field can be spaced at about twice the separation for the same detection performance as a field of similar sonars operated monostatically. That is, a given area can be covered with about one quarter the number of sensors. Centralising the tracking allows about an additional third increase in sonar separation.

RELEASE LIMITATION

Approved for public release

Published by

Maritime Operations Division
DSTO Defence Science and Technology Organisation
PO Box 1500
Edinburgh South Australia 5111 Australia

Telephone: (08) 7389 5555
Fax: (08) 7389 6567

AR 015-022
June 2011

APPROVED FOR PUBLIC RELEASE

Simple Detection-Performance Analysis of Multistatic Sonar for Anti-Submarine Warfare

Executive Summary

Multistatic active sonar has long been promoted as a route to improved performance in anti-submarine warfare. However, it has proven difficult to quantify the benefits of multistatics in operational terms. When is it useful and when is it not worth the effort? This report introduces a simple high-level analysis that tackles this question directly.

We work from the point of view that operators are familiar with monostatic sonar; they know what to expect by way of detection performance in that mode of operation. The method proposed here translates monostatic detection range into multistatic detection performance. From this, we can obtain the separation between multistatic sensors that gives the same detection performance as similar monostatic sensors.

The simplicity of the method is achieved only by making many assumptions, such as, for example, the availability of as much communications capacity as may be required. Our attitude to any such assumption is to suppose that all technical obstacles have been overcome and to ask: what then is the tactical benefit of multistatics, in quantitative terms? If it is potentially substantial, then this may provide a motivation to work on the technical difficulties.

To give a direct comparison between monostatics and multistatics, we adopt a field layout of collocated source–receiver pairs arranged on a triangular grid. We consider large sensor fields only; conclusions may be different if a search area is small enough to be covered with a few sensors.

Detection range is measured by track-initiation probability rather than detection probability. This allows us to compare monostatics and multistatics on an equal footing, as well as allowing comparison of different networking architectures. We consider the two simplest architectures: each receiver performing its own tracking and receivers passing detection information to a central tracking node.

The results show that networking, whether to centralise tracking or to perform multistatics, gives very little advantage when the monostatic p_d curve is close to a cookie cutter. This has long been understood, but a quantitative demonstration has not been presented before, to our knowledge. On the other hand, a p_d curve with a long low-probability tail gives the opportunity for significant multistatic advantage: sonobuoys can be placed at roughly twice the separation if operated multistatically compared with monostatic operation. That is, a given search area could be covered with about one quarter the number of buoys. This applies to both types of tracking architecture, with centralised tracking giving about a further third increase in sonar separation over distributed tracking.

In situations where the false-track rate is insupportably high for fully networked operation, our results show that switching to distributed tracking brings less of a performance penalty than switching to monostatic operation. That is, when multistatic centralised cannot be done, multistatic distributed is better than monostatic centralised.

This page is intentionally blank

Authors

M.P. Fewell
Maritime Operations Division

Matthew Fewell joined DSTO in 2001, coming from an academic physics background. He has worked and published in experimental nuclear structure physics, gaseous electronics, atom–photon interactions including coherent effects, laser physics, plasma processing of materials, the conceptual underpinnings of network-centric warfare and its modelling (including cognitive issues), human-in-the-loop experimentation, and weapon–target allocation in ship air defence. He is at present engaged in anti-submarine warfare operations research, with a focus on networking effects and multi-platform operations.

S. Ozols
Maritime Operations Division

Sylvia Ozols took up a summer vacation scholarship at DSTO in 2009/10. She had just completed her third year in a Bachelor of Mathematics & Computer Science at the University of Adelaide with the intention of going on to postgraduate study in Pure Mathematics.

This page is intentionally blank

Contents

1. INTRODUCTION 1
1.1 Study Question and Scope 2
1.2 Back-of-an-Envelope Analysis of Sonar Detection Performance 3
1.2.1 Monostatic with Definite-Range Law 3
1.2.2 Relating Monostatic and Multistatic Ranges 4
1.2.3 Limitations for Treating Multistatic Networks — the Way Forward 5
1.3 Summary — Interpreting the Study Question 8

2. METHOD 8
2.1 Models of Monostatic Detection 8
2.2 Multistatic Detection Probability 9
2.2.1 Effect of the Absorption Correction 10
2.2.2 Blind Zone 11
2.3 Coverage Area Based on Track-Initiation Probability 12
2.3.1 Track-Initiation Probability for a Single Sonar 13
2.3.2 Network Architecture and Field Track-Initiation Probability 14
2.4 Measure of Performance 16

3. RESULTS 17
3.1 Summary of Modelling Paradigm and Parameter Values 17
3.2 Patterns of Field Track-Initiation Probability 17
3.3 Multistatic Advantage for a Field of Collocated Sources and Receivers 18

4. SUMMARY, COMMENTS AND CONCLUSION 21

ACKNOWLEDGEMENT 22

APPENDIX A: MATHEMATICAL DETAILS 23
A.1. Variants and Properties of the Detection-Probability Models 23
A.1.1 Definite-Range Law and Exponential 23
A.1.2 Fermi Function 23
A.1.3 Tail Width 24
A.2. Some Results from Geometry 25
A.2.1 Cassianian Ovals 25
A.2.2 Ellipses 26
A.3. Field Track-Initiation Probability 27
A.3.1 Listing of Formulae 27
A.3.2 Restriction to Five Pings 30

APPENDIX B: ELABORATIONS OF THE METHOD 31
B.1. Behaviour at Large Source–Receiver Separation 31
B.1.1 Correcting for Absorption 31
B.1.2 Notes on the Absorption Correction 32
B.1.3 Variation in the Spreading Law 33
B.1.4 Near-Field Effects 34
B.2. Bearing-Dependent and Realistic Detection Probabilities 35
B.3. Aspect-Dependent Target Strength 35

APPENDIX C: MATLAB CODE 37
C.1. Bistatic Pair 37
C.2. Field of Collocated Sources and Receivers 41

REFERENCES 47

Figures

Figure 1: Three identical sensors positioned at the vertices of an equilateral triangle 3
Figure 2: Geometry of multistatic detections 4
Figure 3: Elementary results showing the geometry of Cassinian ovals 5
Figure 4: The three p_d curves used as models of monostatic detection performance 9
Figure 5: Effect of the correction for absorption 10
Figure 6: Detail of the behaviour of p_d near the receiver location 11
Figure 7: As in the right column of Figure 5 , but with the inclusion of the blind zone 12
Figure 8: Same as Figure 7(c), but with two values of the pulse-compression factor 12
Figure 9: Relationship between track-initiation probability and detection probability for the 3-in-5 track-initiation rule 13
Figure 10: Comparison of the range dependence of detection and track-initiation probabilities 14
Figure 11: Contours of field track-initiation probability in the interior of a large sonar field for the four network architectures 15
Figure 12: Like Figure 11(d), but showing the region of the central sensor for inter-sensor separations of $2.73\,R_0$ and $2.74\,R_0$ 16
Figure 13: Like Figure 11, but for the Fermi monostatic p_d curve with diffusivity $b = 0.1$ and an inter-sensor separation of $1.9\,R_0$ 18
Figure 14: Like Figure 11, but for the exponential monostatic p_d curve and an inter-sensor separation of $6\,R_0$ 18
Figure 15: Like Figure 14(d), but for inter-sensor separations of $8.1\,R_0$ and $8.2\,R_0$ 19
Figure 16: Values of the measure of performance for the 12 cases calculated 19
Figure 17: Same as Figure 16, but plotted against 'tail width' 20
Figure A1: Definition of the width W_t of the tail region for a Fermi p_d curve 24
Figure A2: Examples of the three classes of Cassinian oval 25
Figure A3: Ellipse 26
Figure A4: Blind-zone behaviour for constant R_b and fixed source–receiver separation R_{SR} 27
Figure B1: As in Figure 6, but with a dotted blue line showing the effect of cylindrical spreading assuming $R_c = R_0$ 34

This page is intentionally blank

Acronyms

CATING	coverage area based on track initiation and no gaps
MOP	measure of performance
SE	signal excess

This page is intentionally blank

1. Introduction

Anti-submarine warfare (ASW) is, and always has been, hard (e.g. [1,2]). The ADF has not given it priority for some time (e.g. [3–5]):

> 'Australian ASW capabilities have been in a state of benign neglect for a couple of decades … Other considerations took precedence over ASW when setting force structure priorities.' [3]

Current developments in submarine technology are likely to make ASW harder [6–8], while the on-going proliferation of capable submarines in our region (e.g. [3,9]) suggests that we may want to be better at it. This situation, coupled with the nature of military leadership, makes it natural that visions for the way forward will be promulgated; but how to assess them? There is a dearth of actual combat experience—the last hot ASW campaign of any significant length took place during World War 2 [1,2]—and ASW technologies are complicated.

Multistatic active sonar is an example. It is promoted as a way forward for ASW and it is not simple. There is little operational experience of it on which to found intuition or military judgement, so analysis is needed to help assess whether it is indeed a way forward and, if so, under what circumstances. When might multistatics be useful and when is it not worth the effort? Answering questions like these is hampered by an 'enduring problem in the analysis of multistatic systems …[namely] the lack of (even approximate) closed-form analytical models of detection performance' [10]. This report introduces a high-level yet quantitative model that, though not closed-form, aims to be simple enough to be readily comprehensible by operators.

The concept behind the analysis involves comparing monostatic and multistatic systems. Operators are familiar with the behaviour of monostatic active sonar; we seek to translate this experience and intuition as simply and directly as possible to a 'comparable' multistatic system. As described in the next subsection, the study question is formulated with a sonobuoy field in mind, but the analysis applies to any type of sonar system. We express sonar-system performance in terms of a 'range of the day', which sweeps up all the system, environmental and target details. The key is relating the range achieved by a network of sonars operated multistatically to the range when the same sonars are operated monostatically, a relationship introduced in §1.2.2 and detailed in §2.2. The success of the analysis hangs on the degree to which this relationship, together with the other aspects of the method, is simple enough and accurate enough for the purpose.

The level of simplicity is (and can only be) achieved by making many assumptions, such as, for example, the availability of as much communications capacity as may be required. It is also assumed that methods have been developed to handle the increased false-

detection rate that comes with networking [11–14]. The attitude adopted with any such required assumption is to suppose that all technical obstacles have been overcome and to ask: what then is the tactical benefit of multistatics, in quantitative terms? If it is found to be potentially substantial, then this may provide motivation to work on overcoming the technical difficulties.

The rest of this section elaborates the study question, sets limits on the scope of the study and explores how far the very simplest analysis, using cookie-cutter detection probabilities, can take us. This sets the scene for the analysis proper, the method of which is described in §2. Section 3 gives the results and §4 contains a summary and a statement of conclusions. Mathematical details are largely relegated to appendices, which also contain the MATLAB code used to generate the results.

1.1 Study Question and Scope

The following are cited as reasons for adopting multistatics (e.g. [10,15–24]): compared with a field of sonars operated monostatically, the same field operated multistatically may

- give longer detection ranges
- increase the number of detection opportunities per ping
- allow higher ping-repetition rates
- complicate the tactical situation for the submarine
- where more than one receiver makes a detection simultaneously (or nearly so), allow improved performance in localisation (see [25] for details), classification and tracking
- provide a tactically significant application for passive sonobuoys that would otherwise be of only marginally utility.

To set some bounds on the scope of the work, this report deals only with the first two items, which are linked if one adopts the paradigm that defines 'detection range' in terms of the range dependence of a cumulative detection (or other) probability [26]. The third and last points are treated in a companion report [27]; the fourth and fifth points are left to potential future work.

In formulating the study question, we seek to draw on operator experience with monostatic sonar. It sets a standard; operators know what to expect by way of detection performance from such a system. Hence we frame the study question as:

> What is the spacing between sonars in a multistatic field that gives the same detection performance as a monostatic field of similar sonars?

To make this work, one must explain how to determine whether two sonar fields display the 'same detection performance' and what is meant by 'similar sonars'. These issues are introduced in the next subsection and addressed in detail in §2. Section 3 presents results of applying the method to a field of collocated source–receiver pairs, which was selected for study because, of all possible layouts, it allows the purest comparison between monostatics and multistatics. Companion reports [27,28] present results for other field layouts.

1.2 Back-of-an-Envelope Analysis of Sonar Detection Performance

The purpose of this subsection is to set out as simply as possible the concept on which the analysis is based. We begin by reiterating the simplest model of detection performance, the 'definite-range law', otherwise known as the 'cookie-cutter' detector. This provides a pointer to a simple quantification of multistatic detection performance. The results turn out to be oversimplified, for reasons explained in §1.2.3, but they do lead to some general and robust conclusions on the conditions required for multistatics to be beneficial.

1.2.1 Monostatic with Definite-Range Law

The 'definite-range law', also known as a 'cookie-cutter detector', is the simplest model of detection performance. In its most basic form, the 'ideal definite-range law',[(a)] detection probability p_{d} as a function of range R to the target is

$$p_{\mathrm{d}}(R) = \begin{cases} 1 & \text{if } R \le R_0 \\ 0 & \text{if } R > R_0. \end{cases} \tag{1}$$

The quantity R_0 is the detection range or 'range of the day'. Equation 1 applies to an isotropic detector, that is, one that detects equally well in all directions. Many types of sonobuoy are good examples.

Figure 1 shows three identical cookie-cutter sensors arranged in a triangular array. As shown, the inter-sensor spacing D_{s} is not optimum because there is a region covered by all three sensors; that is, the overall coverage area can be increased without introducing a gap by choosing a somewhat larger D_{s} value. Simple geometry shows that the maximum inter-sensor spacing for which there is no gap in the coverage is

$$D_{\mathrm{s,max}} = R_0\sqrt{3} \approx 1.732\,R_0. \tag{2}$$

This maximum spacing for which there are no gaps provides a simple measure of the detection performance of an array of sensors.

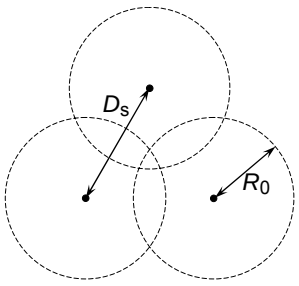

Figure 1: Three identical sensors positioned at the vertices of an equilateral triangle of side length D_s*. The broken lines show the detection ranges* R_0 *of each. The maximum spacing for no gaps in the coverage is found by increasing* D_s *from the value shown in the Figure until the area of common overlap of the three detection-range circles just goes to zero.*

[(a)] For reference, the general form of the definite-range law is given in Appendix A.1.1.

1.2.2 Relating Monostatic and Multistatic Ranges

The transmission-loss term of the sonar equation (e.g. [29(ch.5)]) provides a way of connecting the detection ranges of a field of sonars operated monostatically with the same sonars operated multistatically. In the monostatic case with spherical spreading and neglecting absorption, the transmission loss TL is

$$\mathrm{TL}_{\mathrm{mono}} = 40 \log R \tag{3}$$

in the conventional decibel units. The factor of 40 arises because the acoustic energy traverses the range R twice, once from source to target and a second time from the target back to the receiver that is collocated with the source. The geometry of multistatic detections is shown in Figure 2. Here, the transmission loss is

$$\mathrm{TL}_{\mathrm{multi}} = 20 \log (R_{\mathrm{ST}} R_{\mathrm{TR}}). \tag{4}$$

It is clear that the two transmission losses can be made formally equal by introducing an equivalent monostatic range R_{equiv}:

$$R_{\mathrm{equiv}} = \sqrt{R_{\mathrm{ST}} R_{\mathrm{TR}}}\,. \tag{5}$$

The analysis in this report is based on the concept of using R_{equiv} to reference a monostatic detection-probability curve. That is, if a monostatic p_{d} curve is known for a particular source, collocated receiver, target and environment, then the effect of separating the source and receiver while keeping everything else the same is determined by using R_{equiv} in the monostatic p_{d} curve. This analytical concept is not new; it is implicit in many studies (e.g. [15,30]) and has also been explicitly used elsewhere (e.g. [10,24,31], also [32] for bistatic radar applications). The basic behaviour of the model is illustrated in Figure 3 using the definite range law of Equation (1) as the equivalent monostatic p_{d} curve. The resulting shapes are known as Cassinian ovals (e.g. [33(§53)], Appendix A.2.1).

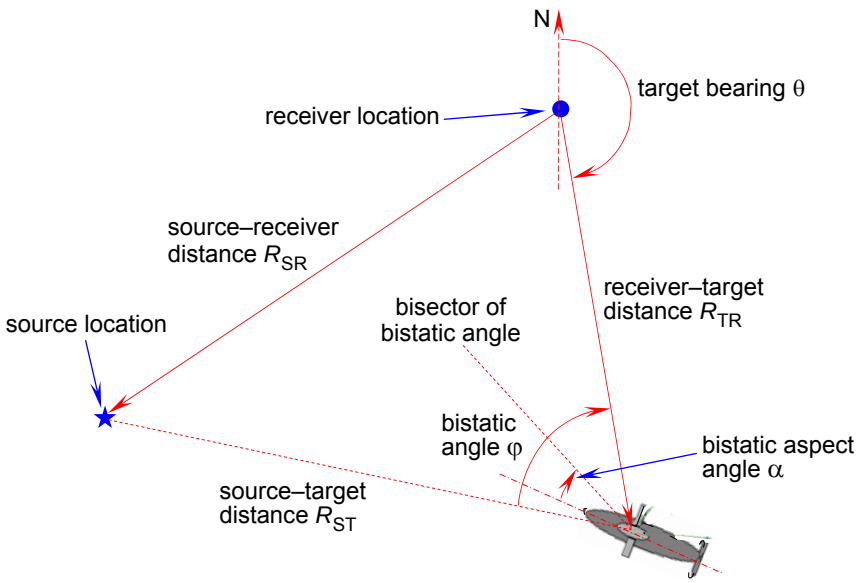

Figure 2: Geometry of multistatic detections. This report uses only the distances, not angles—sources and receivers are assumed to be omnidirectional and the aspect dependence of the target strength is neglected.

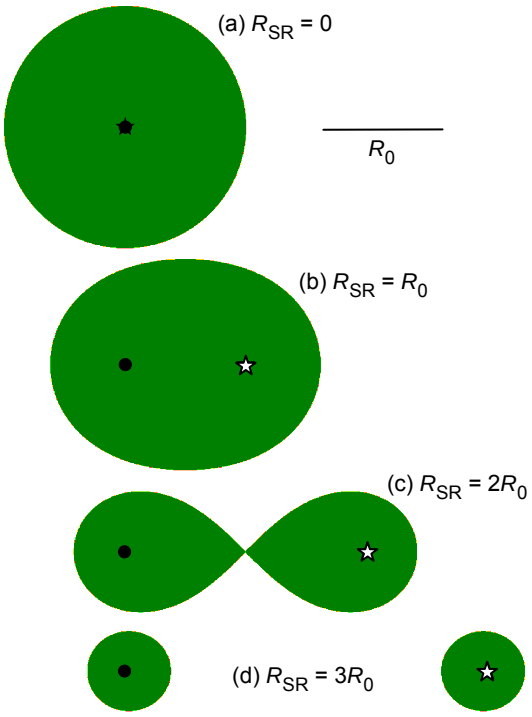

Figure 3: Elementary results showing the geometry of Cassinian ovals – detection coverage areas (green) with a cookie-cutter equivalent monostatic p_d*: (a) monostatic, (b–d) bistatic with source–receiver separation shown. Locations of the receiver are shown with circles and the source with stars. The scale bar shows the length corresponding to the monostatic detection range* R_0.

The method allows study of the effect of 'switching on' multistatics, in the manner implied in the study question of §1.1. It can be applied to any available monostatic p_d curve, whether schematic or the product of acoustic-propagation calculations. Because it is a comparative analysis, the impact of assumptions is diluted: to the extent that they affect the monostatic and multistatic situations equally, their effects cancel.

1.2.3 Limitations for Treating Multistatic Networks — the Way Forward

The above analysis has three features that may make it too simple to be useful. These are:

- use of the ideal definite-range law,
- basing coverage area on single-ping detection curves, and
- a definition of R_{equiv} that goes to zero when the target is located at a receiver.

These issues are discussed in the following paragraphs and ways to overcome them are developed, thereby establishing a basis for the full method described §2.

Use of the Ideal Definite-Range Law

Suppose the sonar field comprises collocated pairs of sources and receivers, and receiver data can be processed either monostatically or multistatically. That is, there is both a source and a receiver at each location in Figure 1, and we can choose whether each receiver records echoes from its own source's pings only, or listens for echoes of pings

originating from from any source. If the monostatic p_d curve is the ideal definite-range law (Eqn 1), then it is clear from Figure 3 that there can be no benefit in operating the field multistatically. This is because p_d is unity inside the detection range and zero outside, so any given sensor needs no assistance for targets located inside its detection range, and can provide no assistance outside its detection range. Benefit from multistatics can arise only if the perfection of Equation (1) is disrupted in some way.[b] Possibilities are:

- Each receiver has a blind zone around it, arising because either the same transducer is used both to transmit and receive, which cannot be done simultaneously, or a receive transducer is swamped by the direct blast from a source transducer.[c] The blind zone is a region of zero p_d stretching from zero range out to a value related to the physical length of the ping (details in §§2.1 and 2.2.2).
- No realistic p_d curve is unity all the way out to the range of the day. Ranges where p_d is less than 1.0 are places where neighbouring sensors with overlapping detection regions can provide mutual support.
- The abrupt boundary to the detection region is also unrealistic. Real p_d curves typically tail off toward zero more or less slowly, and usually not monotonically. The tail region is an area where support is both needed from and can be supplied to neighbouring sensors.

All three mechanisms are taken into account, as described in §2.1.

Method of Defining Coverage Area

Figures 1 and 3 suggest an analysis with a measure of performance related to detection coverage area. However, both figures are drawn using detection ranges derived from single-ping p_d values. As argued elsewhere [12,26], it is better to base a definition of detection range on values of track-initiation probability p_{ti}. (There is no difference between p_d and p_{ti} for a cookie-cutter detector, but the distinction becomes important as one moves to a less extremely simplified detection model.)

Track-initiation probability is defined in terms of a track-initiation rule, which typically specifies a minimum number of successful detections in a given number of consecutive detection opportunities. The concept is discussed and justified in §2.3, and details summarised in Appendix A.3. We use the 3-in-5 track-initiation rule in this report. The full derivation of the equations is given in a companion report [34].

In summary, defining detection range through p_{ti} brings two main benefits over definitions in terms of single-ping p_d [26]:

- It provides a level of recognition of the impact of false detections arising from oceanic noise [35]. ('False' detections of non-target objects are a separate issue.) As

[b] These arguments apply only for the field layout considered in §3, which has sources and receivers deployed as collocated pairs. The effect of separating sources and receivers is dealt with in companion reports [27,28]; it can give multistatic benefit even when the monostatic p_d curve is an ideal definite-range law.

[c] The term 'blast zone' is also used. In this report, we use 'blind zone' to cover both situations.

in an earlier study [12], we do not model noise-induced false detections explicitly, but rather rely on the filtering effect of the track-initiation step to mitigate their effect.

- It provides a means of quantifying the effect of networking sensors. This is important for multistatics, which necessarily involves fields of geographically dispersed sensors. The best way to pool detection information from several receivers is an important question that can be addressed in terms of track initiation; §2.3.2 explains how.

Definition of R_{equiv}

The definition of R_{equiv} in Equation (5), though consistent with the sonar-equation description of spreading loss, has the undesirable feature of going to zero as $R_{\mathrm{TR}} \to 0$. It means that not only is p_{d} high at a receiver but also the value is unaffected by the source–receiver distance. This seems inadequate; an improved description is desirable if a sufficiently simple one can be constructed. The following are possibilities:

- There is always a blind zone near the receiver, which means that $p_{\mathrm{d}} = 0$ for R_{TR} near zero.
- Spreading loss changes from spherical to cylindrical at large enough range. When the source is far from the receiver but the target is close, there would be a difference between the monostatic and multistatic cases, since the spreading loss would be cylindrical both ways for monostatic—assuming the receiver to be shifted to the source location—but cylindrical one way (source → target) and spherical the other (target → receiver) for multistatic.
- Spherical spreading applies in the far field of radiated sound. Close to the target, the spreading will show 'near-field' effects.
- Transmission loss is caused by absorption as well as spreading. The absorption loss involves the sum of R_{ST} and R_{TR}, rather than its product, so behaves differently from the spreading loss.

We examined all these effects. Near-field and cylindrical-spreading effects turn out to be unimportant, for reasons given in Appendix B.1. The blind zone is important and is included in the results of §3, but it is an unsatisfactory resolution of the R_{equiv} problem because

- it introduces factors unrelated in principle to the heart of the issue, such as pulse length and whatever level of pulse compression is obtained through sonar-signal processing, which may be considerable (§2.2.2), and
- it does not address the conceptual problem that p_{d} at a receiver ought to show some dependence on the distance to the source.

Absorption provides the answer, as illustrated in §2.2.1. The net impact on the results of the analysis turns out to be small for the geometry and distance scales of interest here, so the details are relegated to Appendices B.1.1 and B.1.2.

1.3 Summary — Interpreting the Study Question

The analysis of §1.2 suggests that the study question should be interpreted in the following terms:

- 'Similar sonars' means that the performance of the multistatic field is determined by using R_{equiv} as the range in a monostatic detection-probability curve. A correction for absorption can be applied if desired.
- 'Sonar spacing' means the maximum spacing for which the area covered is without holes or gaps.
- The area covered should be defined in terms of track-initiation probability p_{ti}, rather than detection probability p_{d}.

The last two points indicate that 'coverage area' as defined here is different from normal usage. To highlight this, we give it a new name: CATING, for 'Coverage Area based on Track Initiation and No Gaps'.

2. Method

The method of analysis is an extension of earlier work [12] to incorporate multistatics. The measure of performance is the maximum sonar separation consistent with a coverage area without gaps, where coverage area is defined in terms of track-initiation probability p_{ti} (CATING). The use of p_{ti} allows us to quantify the effects of distributed and centralised tracking in a manner consistent with the treatment of multistatics, so that the study question can be addressed for both types of tracking. This is explained in §2.3.2. Before this, §2.1 sets out two simple generalisations of the definite range-law and §2.2 details how this is translated to multistatic sensors. Section 2.4 gives the method of calculating the measure of performance.

2.1 Models of Monostatic Detection

Although the method of relating monostatic and multistatic detection performance can be used with any type of monostatic single-ping p_{d} curve, in this report we use schematic curves, in part to keep the results unclassified, but also in an attempt to cover a reasonable range of detection behaviour with a few curves.

Two classes of functions are used. The first is of the 'Fermi function' type:

$$p_{\text{d}}(R) = \begin{cases} \dfrac{1}{1+10^{(R/R_0-1)/b}} & \text{if } R \geq R_{\text{b}} \\ 0 & \text{if } R < R_{\text{b}}, \end{cases} \tag{6}$$

where

- R_0 is the range of the day, defined as the range at which $p_{\text{d}} = 0.5$,

- b is a 'diffusivity' parameter that describes the 'tailing'; that is, rapidity with which probability values switch from near unity for small R to near zero for large R, and
- R_b is the radius of the blind zone.

This function shows quite a sharp decrease in p_d at ranges around R_0, at a rate that depends on b. As $b \to 0$, it approaches the definite-range law of Equation (1). To explore the influence of the diffusivity parameter on sonar field performance, we performed the analysis twice, using the two values of b shown in Figure 4.

The second class of function used to model p_d behaviour is of a simple exponential type:

$$p_d(R) = \begin{cases} 10^{-0.30103R/R_0} & \text{if } R \geq R_b \\ 0 & \text{if } R < R_b, \end{cases} \tag{7}$$

where the numerical factor is required to ensure that $p_d(R_0) = 0.5$. This function has a much longer 'tail region' where $0.1 \leq p_d \leq 0.5$ than either of the Fermi functions used, as Figure 4 illustrates. On the other hand, it has lower p_d at ranges less than R_0.

The length R_b of the blind zone is related to the physical length of the transmitted acoustic pulse. If the same transducers are used both to transmit and to receive, or if the transmitted waveform does not allow the application of pulse-compression techniques, then echos cannot be received until transmission is complete. It means that the closest detectable object lies at a range equal to half the pulse length. Figure 4 is drawn with $R_b/R_0 = 0.075$, which corresponds to a pulse length of 1.5 km (pulse duration ~1 s) if the range of the day is 10 km.

2.2 Multistatic Detection Probability

It is a foundation of this analysis that the multistatic detection probability is obtained from either Equation (6) or (7), as the case may be, as $p_d(R_{equiv})$, where R_{equiv} is given by Equation (5). There are two provisos: we correct the p_d value for absorption (though the effect is

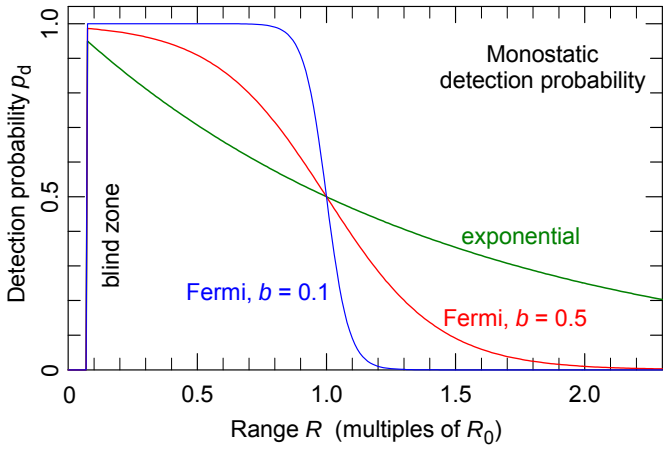

Figure 4: The three p_d *curves used as models of monostatic detection performance. Range is expressed as multiples of the range of the day* R_0.

small), and the treatment of the blind zone is different in the multistatic case; it is not correct simply to compare R_{equiv} with R_b. These two issues are discussed in the following subsections.

2.2.1 Effect of the Absorption Correction

As described in Appendix B.1.1, the absorption correction is applied to a signal excess (SE) rather than directly to a p_d value. Hence, the method of correction requires converting the value of $p_d(R_{equiv})$ to an SE, applying the correction, then converting back to give the $p_{d,corr}$ value.

The effect of the procedure is displayed in Figure 5, where the left column shows uncorrected values—i.e. $p_d(R_{equiv})$—and the right column shows $p_{d,corr}$. In this figure the monostatic p_d values are from the Fermi function with a diffusivity of 0.5, the attenuation coefficient is α = 0.1 dB/km, which is appropriate for an acoustic frequency of about 2 kHz [36], and the range of the day is set to 10 km. The left column of Figure 5 shows the undesirable behaviour discussed in §1.2.3: p_d rises to 1.0[(d)] at the location of the receiver regardless of the source–receiver separation. The right-hand panels show how the correction eliminates the effect: p_d values peak at 0.89 in the bottom right panel. (This is shown more clearly in Figure 6.) It is a rather small effect in view of the large range involved: nine times the range of the day.

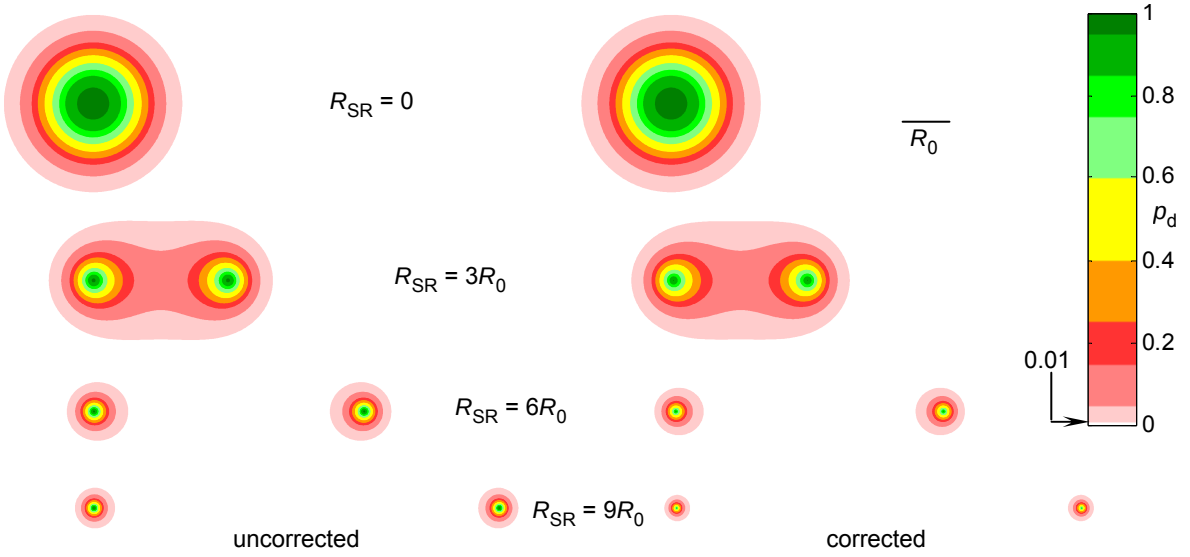

Figure 5: Effect of the correction for absorption: left column – uncorrected; right column – corrected. Contours of detection probability are derived from a Fermi-function monostatic p_d *of diffusivity* b = *0.5 using the source–receiver separations shown, a range of the day of 10 km and an attenuation coefficient of 0.1 dB/km. (The contour fill colour is white below* p_d = *0.01. Source and receiver locations are not marked in the manner of Figure 3 to avoid obscuring* p_d *values in their immediate vicinity.)*

(d) The peak is actually 0.9901, because that is the value of the Fermi function (Eqn 6) at R = 0 when b = 0.5. (This point is discussed in Appendix A.1.2.)

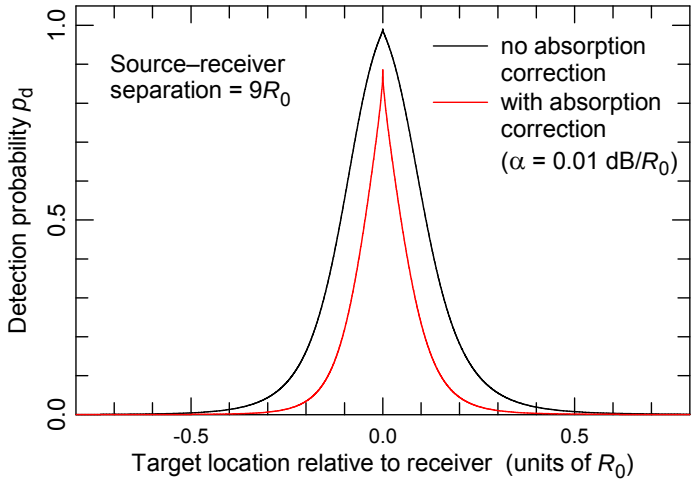

Figure 6: Detail of the behaviour of p_d *near the source or receiver location in the two bottom panels of Figure 5.*

2.2.2 Blind Zone

In the monostatic case, the blind zone is circular with a radius R_b equal to half the transmitted pulse length. The same principle applies for a multistatic geometry, but the separation between source and receiver gives the blind zone an elliptical shape. That is, target locations such that

$$R_{ST} + R_{TR} < R_{SR} + 2R_b \tag{8}$$

cannot be detected because their echoes arrive at the receiver at the same time as some portion of the pulse directly from the source. Expression (8) with the inequality replaced by an 'equals' sign defines an ellipse with foci at the source and receiver and the shortest distance from either equal to R_b. Figure 7 shows some examples. This figure contains an important message: the dramatic increase in the size of the blind zone as the source–receiver separation increases. Though entirely consistent with the geometry of ellipses (see Appendix A.2.2), it nevertheless appears to be a significant negative for multistatics.

The large size of the piece taken out of the covered area by the blind zone, so apparent in Figure 7, provides a motivation for seeking ways around it. For example, it is possible to design a pulse waveform so that careful signal processing can separate an echo from a partly overlapping direct blast, thereby reducing the $2R_b$ term by a 'pulse-compression factor'. This has the effect of increasing the eccentricity of the ellipse, which means reducing its minor axis (Appendix A.2.2). In other words, the ellipse shrinks toward the source–receiver line. The effect is illustrated in Figure 8, to be compared with Figure 7(c), which shows the same conditions without pulse compression. The theoretical maximum value of the pulse compression factor is the pulse duration multiplied by the pulse bandwidth [15], a product that can in practice exceed several hundred.

The benefits of pulse compression seem clear, but are in fact marginal for the field geometry studied in §3, because the monostatic capability that comes with collocated source–receiver pairs largely covers the multistatic blind zones. For this reason, we do not consider the possibility of pulse compression in the rest of this report.

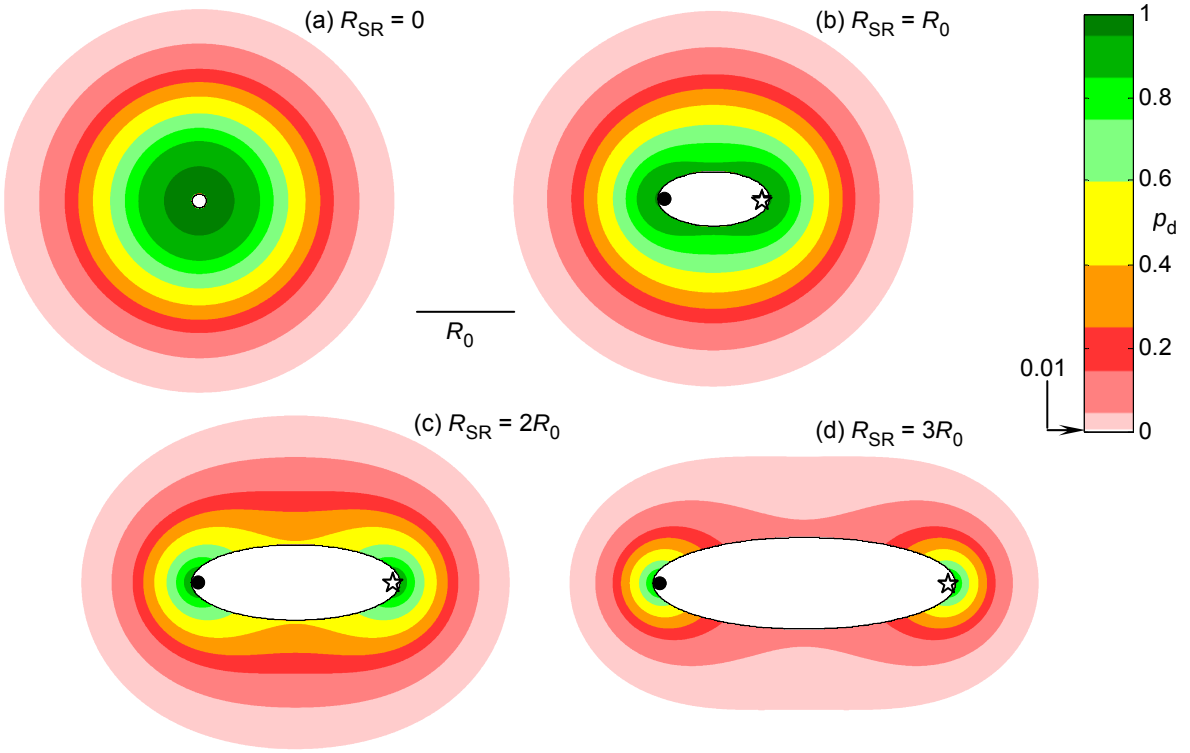

Figure 7: As in the right column of Figure 5 , but with the inclusion of the blind zone, which is delineated with a thin black line. Locations of the receiver are marked with circles and the source with stars, except in panel (a), where the markers would obscure the blind zone.

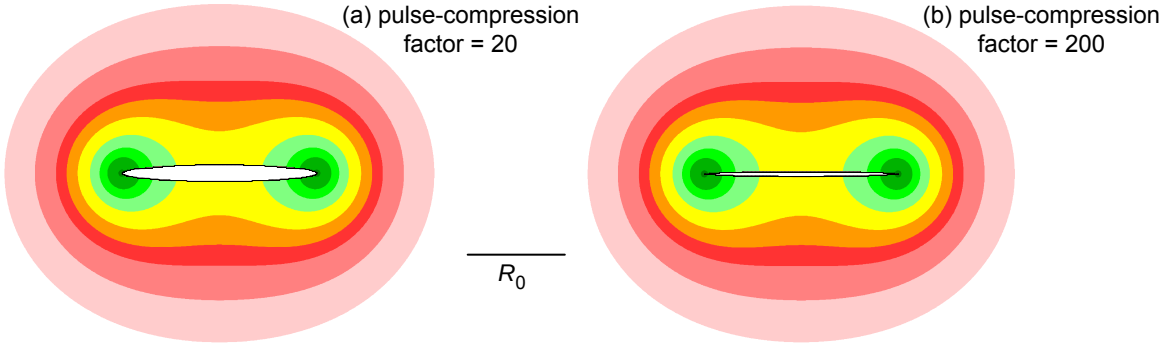

Figure 8: Same as Figure 7(c), but with two values of the pulse-compression factor (and without the node markers).

2.3 Coverage Area Based on Track-Initiation Probability

We consider a track-initiation rule of the type: start a track if there are at least m detections in n consecutive opportunities.[e] This is straightforward for a single monostatic sonar, as

[e] There are other types of rule (e.g. [37,38]), some of which theoretically give a lower rate of false track initiation. However, m-in-n rules remain in widespread use operationally.

outlined in §2.3.1, but questions arise with networks of sensors. If there are many sources, how should one count detection opportunities—is it n pings from one source, the next n pings from any source, or n pings of each source? We adopt the last, for reasons briefly summarised in §2.3.2 and detailed in a companion report [34]. When the field has many receivers, does each perform its own tracking, or is detection information pooled at a central tracking node? Should the answer to this question depend on whether the field is operated multistatically or not? Exploration of these two questions is central to the analysis in this report.

2.3.1 Track-Initiation Probability for a Single Sonar

We restrict our attention to the 3-in-5 track initiation rule. That is, we require the probability of making three or more detections in five consecutive opportunities. If all five opportunities have the same p_d value and are statistically independent, then the track-initiation probability p_{ti} is [12]

$$p_{ti} = {p_d}^3\left(10 - 15p_d + 6{p_d}^2\right). \tag{9}$$

This equation is plotted in Figure 9, showing that p_{ti} is less than p_d when $p_d < 0.5$ and greater than p_d for large p_d values. The effect on the probability–range curves is to steepen the transition from high to low probability values, as illustrated in Figure 10. In the Fermi-function case, the effect of using p_{ti} is similar to using a p_d with lower diffusivity, as the blue dotted curve in Figure 10(b) shows.

The p_{ti} used here is the 'local' p_{ti} of reference 26. It is preferred to a cumulative p_{ti} because a scenario is needed to calculate cumulative p_{ti}, which is unnecessarily restrictive in the present context. Also, we consider the 3-in-5 rule only; some insight into the effect of choosing other values of m and n is given elsewhere [12,34].

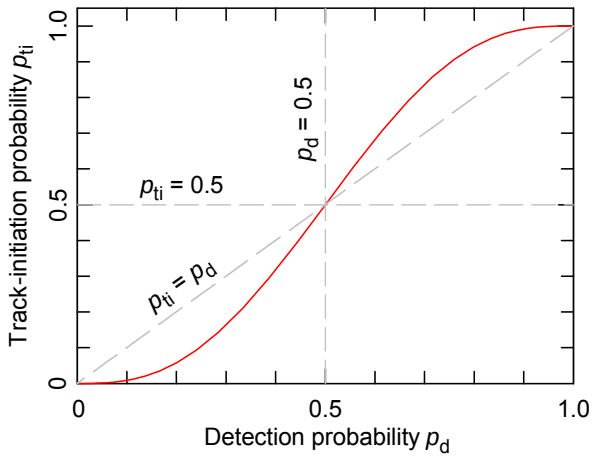

Figure 9: Relationship between single-sensor track-initiation probability and detection probability for the 3-in-5 track-initiation rule.

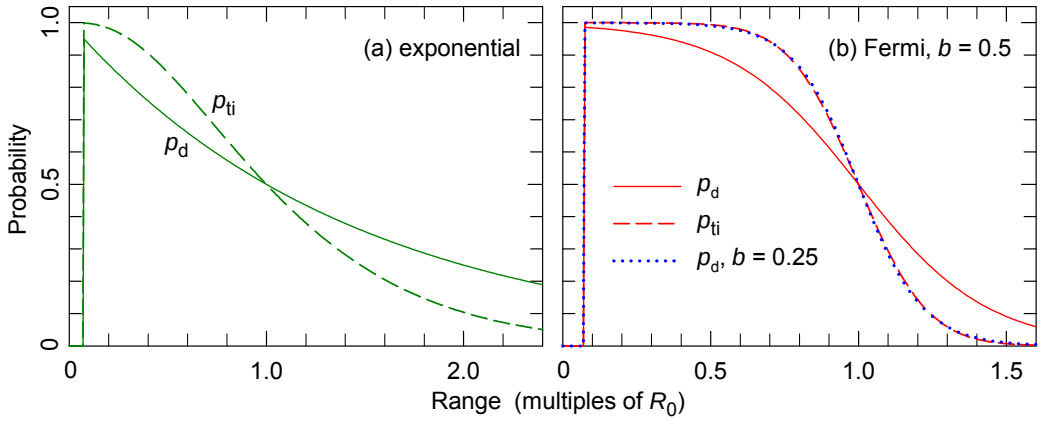

Figure 10: Comparison of the range dependence of detection probability (full lines) and track-initiation probability (dashed lines) for (a) exponential p_d*, (b) Fermi-function* p_d *with* b = *0.5. The blue dotted line in panel (b) shows a Fermi-function* p_d *with* b = *0.25.*

2.3.2 Network Architecture and Field Track-Initiation Probability

In applying the 3-in-5 rule to a networked field with many sources, one must address the question: what constitutes 5 detection opportunities? Our view, that the answer should be 5 pings of every source in the field, is argued in detail in a companion report [34]. In summary, we take the point of view that the networking ought not to interfere with the detection processing of the sonars. Each sonar processes its acoustic data in the same manner whether the field is networked or not. The difference lies in how the resulting detections are handled. As discussed in reference 34, we consider four types or 'architectures' of sonar network:

- *Monostatic with distributed tracking*: The sonars operate independently of each other. Each sonar comprises a source–receiver pair and each performs its own tracking based solely on detections from its own pings. A given sonar must ping at least 3 and up to 5 times before it knows whether to start a track. Any data fusion that may occur consists in passing information on initiated tracks. This is the baseline system.
- *Monostatic with centralised tracking*: Each receiver continues to respond only to echoes from its own source, but detection information is passed to a central tracking node. Each source still pings five times, so that, in effect, the track-initiation rule becomes 3-in-5J for a field comprising J sonars.
- *Multistatic with centralised tracking*: Each receiver in the field processes echoes from any source, not just its own, with detection information being passed to a central tracking node. Each ping produces, in principle, J detection opportunities for a field of J receivers. If there are also J sources, each of which pings 5 times, then the track-initiation rule is effectively 3-in-5J^2. Also, if there are 3 or more receivers in the field, then it is possible to initiate a track on a single ping.
- *Multistatic with distributed tracking*: It is possible that tbe false-alarm rate at the central tracking node in the centralised multistatic architecture may be insupportably high. In an attempt to mitigate this, it has been suggested that a multistatic field could return to distributed tracking [37,39]. That is, each receiver operates multistatically but does its own tracking. With 5 pings from each of J

sources, this returns the track-initiation rule to 3-in-5*J*. Hence, this architecture should, at first sight, show similar sensitivity to the false-detection rate as a monostatic field with centralised tracking.

To provide a basis for quantifying the detection performance of fields of sensors in a way that treats different architectures on an equal footing, we need to generalise the concept of track-initiation probability in §2.3.1 to encompass the whole field. The required mathematical derivations are detailed in reference 34, with results listed in Appendix A.3.

Figure 11 displays the impact of network architecture. The centralised multistatic case (panel d) has field track-initiation probability $p_{\mathrm{ti,f}}$ exceeding 0.75 over the whole area shown (more than 0.85 over most of the area), whereas the distributed monostatic case in panel (a) shows many regions with $p_{\mathrm{ti,f}}$ below 0.15.

The comparison between centralised monostatic and distributed multistatic cases in panels (b) and (c) is interesting in view of the argument above that these two should have similar sensitivity to false detections. For the conditions shown in Figure 11, the distributed multistatic architecture clearly performs better, in the sense that the $p_{\mathrm{ti,f}}$ values between the sensors remain above 0.4 everywhere in Figure 11(c), but fall below 0.25 in several places —the red patches— in Figure 11(b).

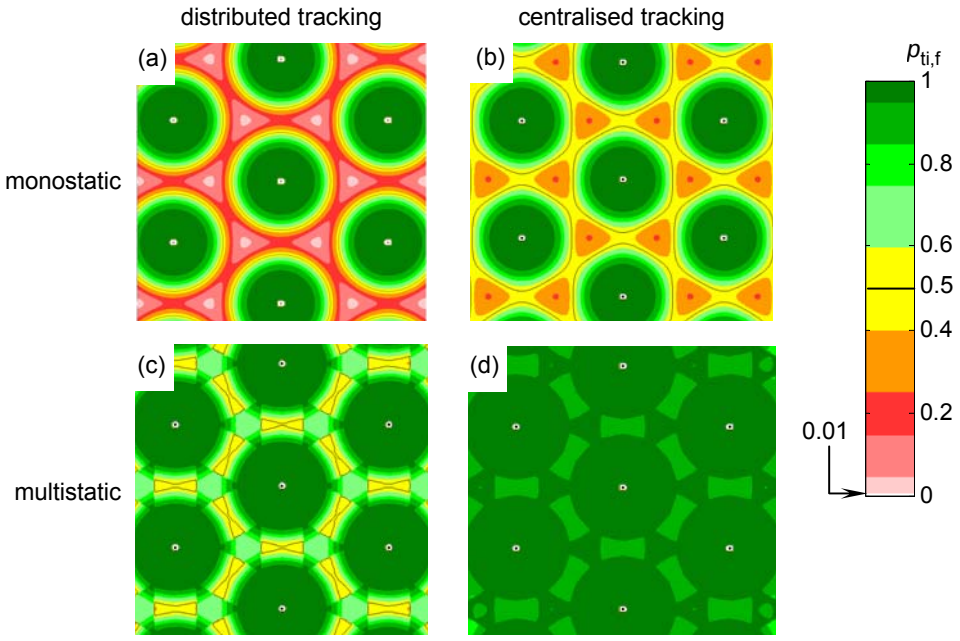

Figure 11: Contours of field track-initiation probability in the interior of a large sonar field for the four network architectures. The field comprises posts (collocated source–receiver pairs), indicated by the small dots at the centre of each monostatic blind zone, on a triangular grid spaced at 2.5 times the range of the day. The monostatic p_d *curve is a Fermi function with diffusivity b = 0.5 and the absorption correction is applied to the multistatic cases. The effect of the multistatic blind zones is discernable in panels (c) and (d) as sharp-edged structures in the lower-*$\mathrm{p}_{ti,f}$ *regions between the sensors, though it is combined with the range dependence of* $\mathrm{p}_{ti,f}$*. The* $\mathrm{p}_{ti,f}$ *= 0.5 contour is delineated; in (d),* $\mathrm{p}_{ti,f}$ *is nowhere less than 0.75 over the area shown.*

2.4 Measure of Performance

In view of the study question (§1.1) and its interpretation (§1.3), the measure of performance (MOP) adopted is the maximum separation between sensors such that $p_{ti,f}$ is not less than 0.5 in the interior of a large field. Thus, the sensors in Figure 11(d) are too closely spaced; those in all the other panels of Figure 11 are too far apart. To determine the MOP value in a given case, the inter-sensor spacing is adjusted manually until $p_{ti,f} = 0.5$ contours just appear in between the central sensor and the ring of sensors around it, as illustrated in Figure 12. We carried out this procedure to the nearest $0.1\,R_0$ for the exponential p_d curve and the nearest $0.01\,R_0$ for the Fermi-function cases like Figure 12.

In determining an MOP value, The monostatic blind zone is excluded from the requirement that $p_{ti,f}$ be not less than 0.5. That is, a small region of zero $p_{ti,f}$ surrounds each sensor, as shown in Figure 12. We do not reduce the inter-sensor spacing so far as would be required to fill this in.

As emphasised in the next section, the analysis is intended to apply to large-area search only. The implication for MOP determination is that we must use fields extensive enough for there to be no edge effects near the central sensor. For example, edge effects appear in Figure 11(d) as the very small pale-green patches in the corners of the panel. These lie well away from the central sensor. No edge effects are discernable in Figures 11(a–c). In each case analysed, we checked for edge effects by adding successive rings of sensors until $p_{ti,f}$ values in the vicinity of the central sensor were unaltered by the new ring of sensors. More rings of sensors are needed for the exponential monostatic p_d curve than the cookie-cutter (low-diffusivity Fermi), as could be expected.

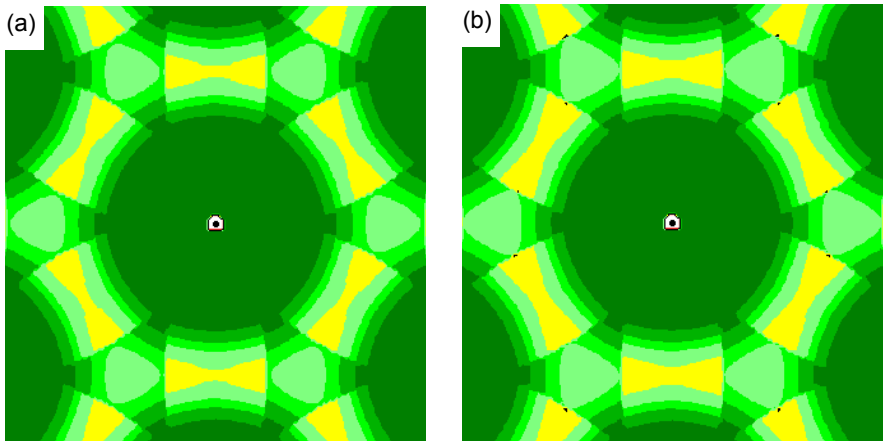

Figure 12: Like Figure 11(d), but showing the region of the central sensor for inter-sensor separations of (a) 2.73 R_0 *and (b) 2.74* R_0*. The small black dots on the edges of the yellow areas in (b) show regions where* $p_{ti,f}$ *just falls below 0.5.*

3. Results

For convenience, we first collect all the assumptions and parameter values used, then show examples of the patterns of $p_{\mathrm{ti,f}}$ and present the results.

3.1 Summary of Modelling Paradigm and Parameter Values

- *Study question*: What is the spacing between sonars in a multistatic field that gives the same detection performance as a monostatic field of similar sonars?
- *Field layout*: Triangular, as in Figure 11, with a post (collocated source–receiver pair) at each sensor location.
- *Network architectures* considered:
  - *monostatic distributed*: Each receiver responds only to echoes of pings from its collocated source, and each receiver performs tracking based only on its own detections. This is the baseline case.
  - *multistatic distributed*: Receivers register echoes of pings from any source, but each receiver still performs its own tracking.
  - *monostatic centralised*: Each receiver responds only to echoes of pings from its collocated source. Detection information is passed to a central tracking node.
  - *multistatic centralised*: Receivers attempt detections on every ping and pass the information to a central tracking node.
- Models of *monostatic detection probability vs. range curves*:
  - Fermi, $b = 0.1$,
  - Fermi, $b = 0.5$, and
  - exponential.

  All are parametric in R_0, the range of the day, so this need not be specified.
- *Multistatic detection probability*: From monostatic p_{d} curves using $R_{\mathrm{equiv}} = \sqrt{R_{\mathrm{ST}} R_{\mathrm{TR}}}$.
- *Absorption correction*: Applied using:
  - attenuation coefficient of 0.01 dB per R_0, and
  - noise standard deviation of 8 dB.
- *Blind zone*: Applied using:
  - transmitted pulse length of 1.5 km, taken to be $0.15R_0$ (hence $R_{\mathrm{b}} = 0.075R_0$), and
  - no pulse compression.
- *Measure of performance*: maximum inter-sensor separation such that field track-initiation probability in the interior of a large sensor field is nowhere less than 0.5, except for the residual blind zones in the immediate vicinity of each sensor.

3.2 Patterns of Field Track-Initiation Probability

Figure 11 shows patterns of $p_{\mathrm{ti,f}}$ for the case of Fermi, $b = 0.5$. Corresponding results for the other two monostatic p_{d} curves are shown in Figures 13 and 14. In Figure 13, the monostatic p_{d} curve is close to a cookie cutter, so the networking benefit is small, as suggested in §1.2.3. Figure 14 shows the opposite extreme: the monostatic p_{d} curve has a long tail where p_{d} lies in the range ~0.1–0.5, which is the best situation for gaining advantage through

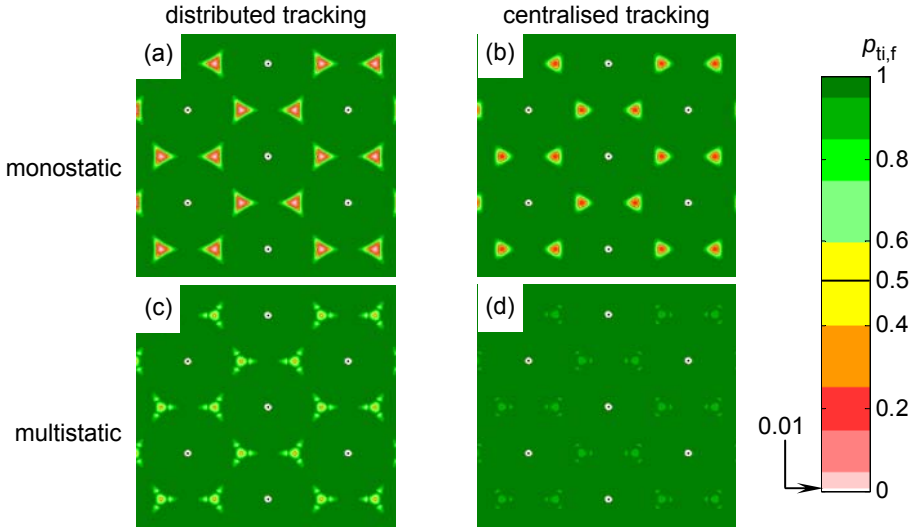

Figure 13: Like Figure 11, but for the Fermi monostatic p_d *curve with diffusivity* b = *0.1 and an inter-sensor separation of 1.9* R_0

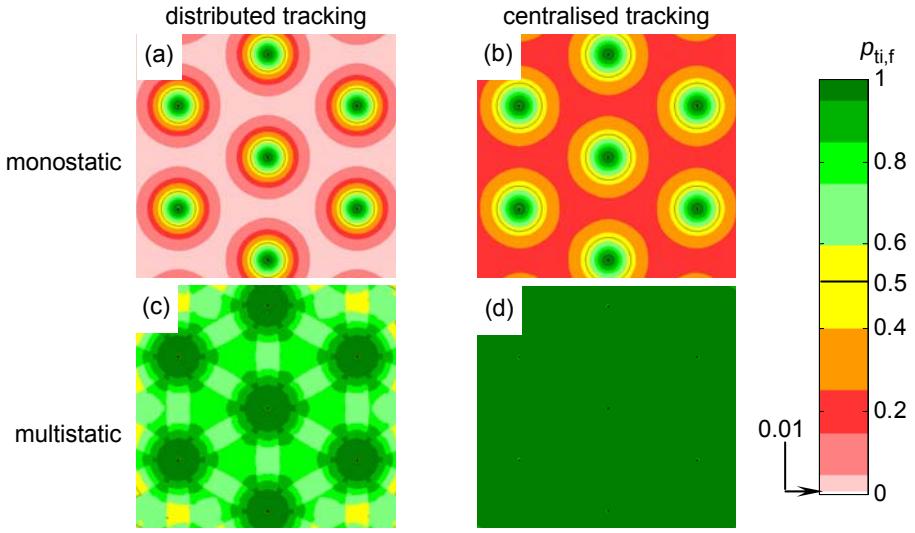

Figure 14: Like Figure 11, but for the exponential monostatic p_d *curve and an inter-sensor separation of 6* R_0

networking [12]. Figure 14(d), the multistatic centralised case, has $p_{ti,f}$ over 0.95 everywhere, apart from in the residual blind zones, so the sensors can be spaced much further than the $6\,R_0$ shown. Figure 15 illustrates the determination of the maximum spacing for this case.

3.3 Multistatic Advantage for a Field of Collocated Sources and Receivers

The results of the analysis are presented in Figure 16. The quantitative performance gain in operating the field multistatically can be gauged by comparing a blue bar with the red bar

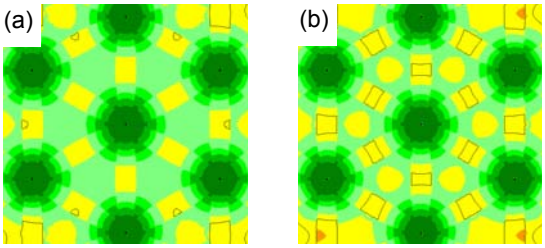

Figure 15: Like Figure 14(d), but for inter-sensor separations of (a) 8.1 R_0 *and (b) 8.2* R_0*. The regions with* $p_{ti,f}$ *below 0.5 in panel (a) are due to edge effects.*

to its left. The inter-sonar separation of $\sqrt{3}\,R_0$ appropriate for a cookie-cutter p_d curve is shown for comparison.

The left-most group of bars in Figure 16 relate to a monostatic p_d curve that is almost a cookie-cutter. The multistatic advantage is very small with distributed tracking (solid bars) and not much larger for centralised tracking (striped bars).

In contrast, the right-most group of bars, for the exponential monostatic p_d curve, show significant multistatic advantage for both tracking architectures. For the centralised architecture (striped bars), the maximum inter-sensor spacing for the multistatic field is a little under double that of the monostatic field (8.1 R_0 cf. 4.8 R_0) and for distributed tracking it is more than double, at 6.3 R_0 compared with 2.8 R_0. As to the impact of tracking architecture, for both monostatic and multistatic fields centralised tracking does about a third better than distributed tracking. In summary, using the monostatic distributed configuration as a baseline, moving to multistatics approximately doubles the field performance metric and centralising the tracking increases it by about another third.

The middle group of bars show a case of a monostatic p_d curve that is clearly not a cookie cutter, but with a tail region of relatively limited extent. Multistatic advantage is present but modest. This time, again starting with the monostatic distributed baseline, moving to

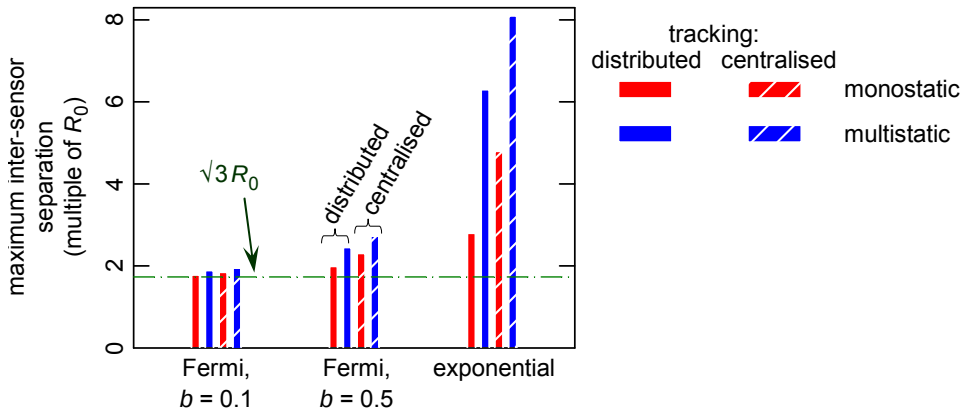

Figure 16: Values of the measure of performance for the 12 cases calculated. Each pair of red and blue bars shows the multistatic advantage for that combination of monostatic p_d *curve and tracking architecture. The baseline network configuration is monostatic with distributed tracking, shown as the left-most bar in each of the three groups.*

multistatics increases the performance metric by about 20% and centralising the tracking adds something over another 10%.

The magnitude of the tailing in the monostatic p_d curve can be quantified by 'tail width' W_t, which we define as the distance from the range at which $p_d = 0.5$ to the range at which $p_d = 0.1$ (Appendix A.1.3). Figure 17 shows the data of Figure 16 plotted against tail width. The extent to which the exponential represents extreme behaviour is apparent. It is also clear that multistatic advantage, which is the difference between corresponding red and blue curves, grows with increasing tail width. There is no such advantage, nor any advantage in centralising detections for the purpose of tracking, for a monostatic p_d curve with zero tail width, such as a cookie cutter.(f)

A separate question concerns the relative performance of the centralised monostatic and distributed multistatic architectures (middle two bars of each group in Figure 16 or middle two lines in Figure 17). This becomes interesting if, for some reason, one cannot cope with the false-track rate of the fully networked case. In such a situation, is it better to give up centralised tracking or multistatics? In every case examined, distributed multistatics outperforms centralised monostatics, as Figure 17 makes clear, though the difference is marginal if the tail width is small. Other considerations, such as the high sensitivity of a multistatic field to sonar positioning errors, may cause monostatics to be favoured in some situations.

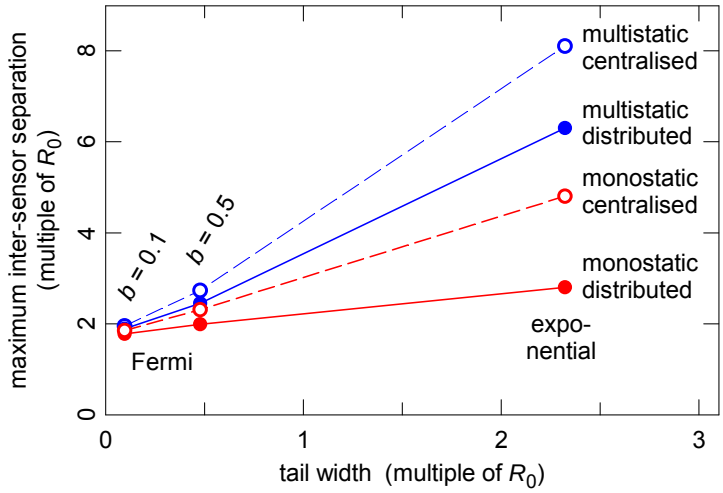

Figure 17: Same as Figure 16, but plotted against tail width – the distance between the range at which $p_d = 0.5$ *and the range at which* $p_d = 0.1$ *(Appendix A.1.3). The definite-range law ('cookie-cutter') has zero tail width. All curves converge to a maximum inter-sensor spacing of* $\sqrt{3}R_0$ *(~1.73* R_0*) as the tail width goes to zero.*

(f) This conclusion applies only for the ideal definite-range law of Eqn (1), where there is detection certainty inside the detection range. If p_d is not 1.0 inside the cookie cutter (e.g. as in Appendix A.1.1) then networking will bring an advantage even zero tail width. Reference 12 contains an example. See also the comments in footnote (b): multistatic advantage can also be obtained in environments with zero tail width by separating the sources and receivers, or adding extra receivers to a field of posts.

4. Summary, Comments and Conclusion

This report describes a modelling method for comparing the detection performance of a field of multistatic sonar systems with that of a field of similar sonars operated monostatically. The basis of the method is the sonar-equation description of transmission loss due to spreading, which leads to a very simple connection between the multistatic ranges and an equivalent monostatic range:

$$R_{\text{equiv}} = \sqrt{R_{\text{ST}} R_{\text{TR}}} \,.$$

It means that multistatic detection probabilities can be obtained directly from monostatic p_{d} values. The modelling paradigm supposes that the monostatic p_{d} values are known *a priori*, so the comparison is straightforward. For simplicity and to keep the study unclassified, we use three simple monostatic p_{d} curves: one that is almost a cookie cutter, one with a long tail where p_{d} lies in the range ~0.1–0.5, and a third intermediate case.

The form of the sonar equation leading to the above definition of R_{equiv} applies in the noise-limited regime. Acoustic-propagation calculations for the reverberation-limited regime show as much regularity as when noise-limited (e.g. Fig. 7 in ref. 30), so an analysis along the lines of the analysis presented in this report should be possible by starting with the reverberation-limited form of the sonar equation (e.g. [11]). Of course, the details would, and conclusions might, be different from those presented here.

The results reported in §3.3 include the effect of the blind zone between source–receiver pairs and a correction for the effect of transmission loss due to absorption, using a value of the attenuation coefficient appropriate to a sonar frequency of ~2 kHz, although both turn out to be minor given the chosen field layout. Other potential corrections—near-field effects and the effect of a transition from spherical to cylindrical spreading—were investigated and found to be negligible.

To give the most direct comparison possible between monostatics and multistatics, we adopted a field layout of collocated source–receiver pairs ('posts') arranged on a triangular grid with equal spacing between each post. We considered large sensor fields only; conclusions may be different for a search area small enough that it can be covered with a few sensors. For example, Travaglione and Forward consider a single source surrounded by a circle of 2–5 equally spaced receivers [31]. They find an optimum source–receiver spacing of ~$1.3R_0$, but their analysis differs from ours in more than just the field layout: they base their coverage-area metric on p_{d} rather than p_{ti} and they assume very short acoustic pulses (50 ms), so that the blind-zone areas are relatively small.

Aspect-dependent target strength could be included in the present analysis in a similar manner to the absorption correction. We have not investigated this. Although the possibility of 'glint' detections is held to be an advantage of multistatics over monostatics, the effect is probably not as significant when sources and receivers are collocated compared to when they are separated, particularly if the submarine CO is aware of (or has a shrewd guess at) the layout; for then, in addition to knowing the locations of the sources, he or she also knows where all the receivers are.

Perhaps the most significant shortcoming of the analytical method is the neglect of time, a feature that is typical of methods based on coverage area. We take no account of the time required for five pings from all sources in the field, nor of submarine motion during this time. On the plus side, it allows us to avoid the difficult issue of ping sequencing (which others have considered [40,41]), but this scarcely compensates for the negatives that the approximation entails. The best hope for mitigating its effects may be future technical developments that render its impact less significant, such as methods for allowing simultaneous pings by several sources (e.g. [40]), or continuous active sonar (e.g. [42–44]), which would eliminate the need for ping sequencing altogether.

The measure of performance is the maximum inter-sensor spacing such that the field track-initiation probability between sensors is not less than 0.5. The use of track-initiation probability fills two purposes:

- Since track initiation acts as a false-detection filter, use of $p_{\mathrm{ti,f}}$ provides some level of robustness against the effect of false detections, which otherwise are not considered in this analytical method.
- It provides a way of quantitatively comparing the performance of different network architectures, both monostatic versus multistatic, and also distributed versus centralised tracking.

It should be carefully noted that the measure of performance relates to *detection performance only*. We take no account of other issues in multistatics, such as localisation error or the time required to achieve a given level of confidence in the identity of the contact.

The results show that networking, whether to centralise tracking or to perform multistatics, gives very little advantage when the monostatic p_{d} curve is close to a cookie cutter. This has long been understood, but a quantitative demonstration has not been presented before, to our knowledge. On the other hand, the long-tail p_{d} curve gives the opportunity for significant multistatic advantage: with the exponential curve, sonobuoys could be placed at roughly twice the separation if operated multistatically compared with monostatic operation. That is, a given search area could be covered with about one quarter the number of buoys. This is true for both types of tracking architecture, with centralised tracking giving about a third better performance than distributed tracking (Figs 16, 17).

In situations where the false-track rate is insupportably high for fully networked operation, our results show that switching to distributed tracking brings less of a performance penalty than switching to monostatic operation. That is, when multistatic centralised cannot be done, multistatic distributed is better than monostatic centralised.

In terms of providing general conclusions, the field layout considered here is quite restrictive—collocating sources and receivers is perhaps not the best way of employing a multistatic capability. We have extended the analysis to other field layouts, the results of which appear in companion reports [27,28].

Acknowledgement

We thank Drs Z.Y. Zhang and S. Simakov for valuable comments and suggestions.

Appendix A: Mathemaical Details

This appendix collects some results in support of the analysis in the body of the report.

A.1. Variants and Properties of the Detection-Probability Models

A.1.1 Definite-Range Law and Exponential

Equation (1) is referred to as the 'ideal definite-range law'. The general version is

$$p_{\mathrm{d}}(R) = \begin{cases} p_0 & R \le R_0 \\ 0 & R > R_0 . \end{cases} \tag{A1}$$

The only effect of this generalisation is that R_0 does not fulfil our definition of 'range of the day' if p_0 is chosen to be less than 0.5. In such a case there is no range of the day.

In reference 12, the exponential model is written

$$p_{\mathrm{d}}(R) = p_0 \exp\left(-R/a\right). \tag{A2}$$

For p_0 = 1, this gives the same values as Equation (7)—the blind zone aside—if a is set to

$$a = \frac{R_0}{\ln 10 \log 2} = 1.4427 R_0 . \tag{A3}$$

If it is desired to generalise Equation (7) by introducing a p_0 value, then one should write

$$p_{\mathrm{d}}(R) = p_0 10^{-\log(2p_0)R/R_0}, \tag{A4}$$

so that R_0 remains the range of the day (i.e. the range at which p_{d} = 0.5). This formulation requires p_0 > 0.5; for otherwise there is no range of the day. To make Equation (A2) give the same values as Equation (A4), set

$$a = \frac{R_0}{\ln 10 \log\left(2p_0\right)}. \tag{A5}$$

A.1.2 Fermi Function

In reference 12, the Fermi model is written, apart from some minor changes of notation to suit present purposes, as

$$p_{\mathrm{d}}(R) = P_0 \frac{1 + \exp\left(-r_0/a\right)}{1 + \exp\left(\dfrac{R - r_0}{a}\right)}. \tag{A6}$$

(Note that $P_0 \neq p_0$ and $r_0 \neq R_0$, as explained below.) The numerator ensures that $p_d = P_0$ at $R = 0$, but it complicates the interpretation of the r_0 parameter; for the range of the day R_0 is

$$R_0 = r_0 + a \ln\left[2P_0\left(1+e^{-r_0/a}\right)-1\right]. \tag{A7}$$

This cannot be inverted to obtain an expression for r_0 in terms of R_0. In the present report, we choose to drop $(1+e^{-r_0/a})$ factor in the numerator. It means that $p_d(0) \neq p_0$, but the value of $p_d(0)$ is not accessible anyway because the region around $R = 0$ is covered by the blind zone.

Equation (6) can be generalised to include a p_0 factor while retaining the interpretation of R_0 as the range of the day by writing, again apart from the blind zone,

$$p_d(R) = \frac{p_0}{1+10^{\left\{R\left[1+b\log(2p_0-1)\right]-R_0\right\}/R_0 b}}. \tag{A8}$$

It is apparent that this reduces to Equation (6) when $p_0 = 1$. Equation (A8) applies only for $p_0 > 0.5$; for otherwise there is no range of the day. To make Equations (A6) and (A8) give the same values, set

$$r_0 = \frac{R_0}{1+b\log(2p_0-1)}, \qquad a = \frac{b r_0}{\ln 10}, \qquad P_0 = \frac{p_0}{1+10^{-1/b}}. \tag{A9}$$

A.1.3 Tail Width

For the Fermi function, the diffusivity b measures how fast the p_d curve decays to zero at ranges beyond R_0. Another measure of this that is generalisable to other functions is the 'width of the tail region' W_t. Many definitions are possible, but for present purposes it is convenient to define W_t as the distance from R_0—the range at which $p_d = 0.5$—to the range at which $p_d = 0.1$, as illustrated in Figure A1.

For the Fermi function, substitution in Equation (A8) gives

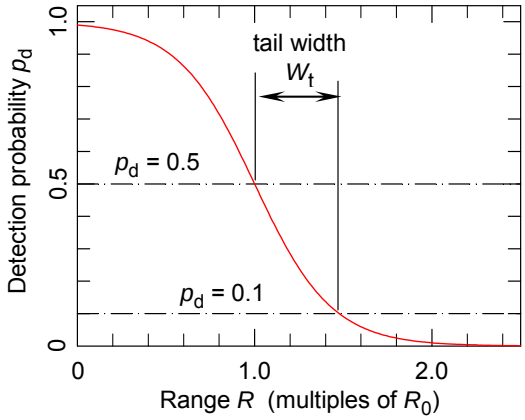

Figure A1: Definition of the width W_t of the tail region for a p_d curve

$$W_t = R_0 b \frac{\log \frac{10p_0 - 1}{2p_0 - 1}}{1 + b\log(2p_0 - 1)}. \tag{A10}$$

For exponentials, substitution in Equation (A4) gives

$$W_t = R_0 \frac{1 - \log 2}{\log(2p_0)}. \tag{A11}$$

Setting $p_0 = 1$ simplifies both these equations very considerably. In the case of the Fermi function, one obtains

$$W_t = R_0 b \log 9 = 0.9542 R_0 b. \tag{A12}$$

That is, W_t is proportional to b. For exponentials, a single value of course results:

$$W_t = R_0 \frac{1 - \log 2}{\log 2} = 2.322 R_0. \tag{A13}$$

A.2. Some Results from Geometry

A.2.1 Cassianian Ovals

A 'Cassinian oval' is the locus of a point moving such that the product of its distances to two fixed points remains constant. That is, in terms of the quantities shown in Figure A2(a), the product $R_{ST} R_{TR}$ is constant. In labelling the examples in Figure A2, we set

$$R_{ST} R_{TR} = {R_0}^2, \tag{A14}$$

corresponding to the 50% probability contour in a coverage plot.

Compilations of the properties of Cassinian ovals are available (e.g. [33(§5.16)]). Their behaviour divides into the three classes shown in Figure A2. For all three, the maximum

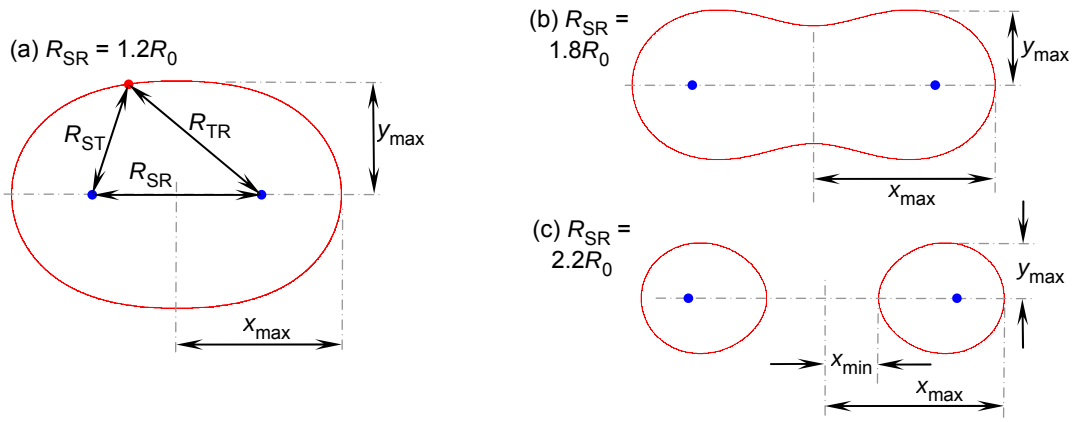

Figure A2: Examples of the three classes of Cassinian oval: (a) $R_{SR} \le R_0\sqrt{2}$, *(b)* $R_0\sqrt{2} < R_{SR} \le 2R_0$, *(c)* $R_{SR} > 2R_0$. *The 'centre' of the oval is the midpoint of the line joining the foci, even if this does not lie within a loop, as in panel (c).*

extent x_{max} of the oval along the line through the foci, measured from the centre, is

$$x_{max} = \sqrt{R_0^2 + R_{SR}^2/4}\,. \tag{A15}$$

The classification of an oval depends on the value of R_{SR} compared with R_0:

- $R_{SR} \le R_0\sqrt{2}$ (Fig. A2a): The oval is similar in appearance to an ellipse. The maximum extent y_{max} from the line joining the foci occurs at the perpendicular through the centre. Its value is

$$y_{max} = \sqrt{R_0^2 - R_{SR}^2/4}\,. \tag{A16}$$

- $R_0\sqrt{2} < R_{SR} \le 2R_0$, (Fig. A2b): The oval remains in one loop, but the maximum extent y_{max} now occurs away from the perpendicular through the centre. Its value is

$$y_{max} = R_0^2/R_{SR}\,. \tag{A17}$$

- $R_{SR} > 2R_0$, (Fig. A2c): The oval has two loops, but the value of y_{max} is still given by Equation (A17). The loops intersect the line joining the foci at $\pm x_{min}$, which is

$$x_{min} = \sqrt{\frac{R_{SR}^2}{4} - R_0^2}\,. \tag{A18}$$

A.2.2 Ellipses

The ellipse is a very well studied curve, but its properties are usually given in terms of the maximum extents, commonly called the major and minor axes—the quantities x_{max} and y_{max} in Figure A3 (e.g. [33(§3.4)]). For present purposes, we need quantities expressed in terms of R_{SR} and the monostatic blind-zone radius R_b, so as to understand the behaviour of the ellipse as these two parameters change.

As is well known, an ellipse is the locus of a point moving such that the sum of its distances to two fixed points remains constant. To represent the blind zone, we write (cf. Eqn 8)

$$R_{ST} + R_{TR} = R_{SR} + 2R_b. \tag{A19}$$

Standard expressions for the properties of the ellipse can be rearranged in favour of R_{SR} and R_b to give

$$x_{max} = R_b + R_{SR}/2, \qquad y_{max} = R_b\sqrt{1 + R_{SR}/R_b}\,. \tag{A20}$$

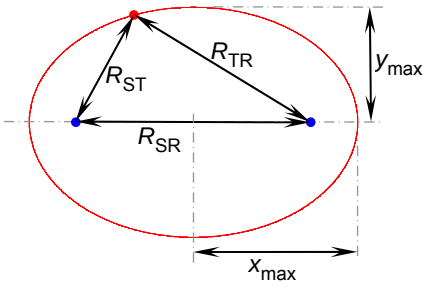

Figure A3: Ellipse

The interesting aspects for understanding the behaviour of the blind zone are the behaviour as

- R_{SR} increases, for constant R_b, and
- R_b decreases, for constant R_{SR};

for the first describes the growth of the blind zone as source and receiver are separated and the second describes the effects of increasing pulse compression at fixed source–receiver separation. These are depicted in Figure A4.

For reference, the eccentricity e of the ellipse is

$$e = \frac{R_{SR}}{R_{SR} + 2R_b}. \tag{A21}$$

An ellipse becomes more circular as $e \to 0$. This corresponds to $R_{SR} \to 0$, i.e. monostatic geometry. As $R_b \to 0$, $e \to 1$, which means that the ellipse becomes more elongated; it collapses toward the line segment joining source and receiver, as illustrated in Figure A4(b).

A.3. Field Track-Initiation Probability

A.3.1 Listing of Formulae

The full derivation of formulae for the field track-probability $p_{ti,f}$ for the various network architectures with the 3-in-5 track-initiation rule is detailed in a companion report [34]. Here the results are listed for convenience.

Monostatic, Distributed Tracking

$$p_{ti,f} = 1 - \prod_{j=1}^{J} \left(1 - p_{ti,j}\right), \tag{A22}$$

where $p_{ti,j}$ is the track-initiation probability of sensor j, given by Equation (9), and J is the total number of sensors in the field.

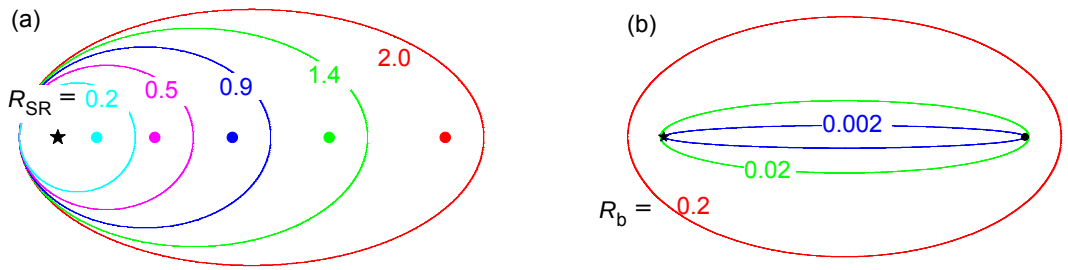

Figure A4: Blind-zone behaviour for (a) constant R_b *= 0.2 and source–receiver separations* R_{SR} *shown and (b) fixed source–receiver separation* R_{SR} *= 2.0 and* R_b *values shown. Source location is marked with a star and receiver location with a circle.*

Monostatic, Centralised Tracking

The field track-initiation probability is written as:

$$p_{\mathrm{ti,f}} = 1 - p(0) - p(1) - p_1(2) - p_2(2), \tag{A23}$$

where, after five pings of each source in the field, $p(0)$ is the probability that there have been no detections anywhere, $p(1)$ is the probability of exactly one detection somewhere in the field, $p_1(2)$ is the probability of exactly two detections by the same receiver and $p_2(2)$ is the probability of exactly two detections, but by different receivers. The expressions are:

$$p(0) = \prod_{j=1}^{J} \left(1 - p_{\mathrm{d},j}\right)^5, \tag{A24}$$

where $p_{\mathrm{d},j}$ is the detection probability for sensor j and J is the total number of sensors in the field,

$$p(1) = 5p(0) \sum_{j=1}^{J} \frac{p_{\mathrm{d},j}}{1 - p_{\mathrm{d},j}}, \tag{A25}$$

$$p_1(2) = 10p(0) \sum_{j=1}^{J} \left(\frac{p_{\mathrm{d},j}}{1 - p_{\mathrm{d},j}} \right)^2 \tag{A26}$$

and

$$p_2(2) = 25p(0) \sum_{j=1}^{J-1} \sum_{j'=j+1}^{J} \frac{p_{\mathrm{d},j}\, p_{\mathrm{d},j'}}{\left(1 - p_{\mathrm{d},j}\right)\left(1 - p_{\mathrm{d},j'}\right)}. \tag{A27}$$

Multistatic, Distributed Tracking

As with the monostatic distributed case, each receiver is first treated separately. The track-initiation probability for receiver k is

$$p_{\mathrm{ti},k} = 1 - p_k(0) - p_k(1) - p_{1,k}(2) - p_{2,k}(2). \tag{A28}$$

The probabilities of zero and exactly one detection after all J sources in the field have pinged five times each are

$$p_k(0) = \prod_{j=1}^{J} \left(1 - p_{\mathrm{d},jk}\right)^5, \tag{A29}$$

$$p_k(1) = 5p_k(0) \sum_{j=1}^{J} \frac{p_{\mathrm{d},jk}}{1 - p_{\mathrm{d},jk}}, \tag{A30}$$

where j enumerates sources and $p_{\mathrm{d},jk}$ is the detection probability for source j and receiver k. The quantity $p_{1,k}(2)$, for which both detections are made on pings from the same source, is:

$$p_{1,k}(2) = 10p_k(0) \sum_{j=1}^{J} \left(\frac{p_{\mathrm{d},jk}}{1 - p_{\mathrm{d},jk}} \right)^2, \tag{A31}$$

and the expression for $p_{2,k}(2)$, for which the two detections involve different sources, is:

$$p_{2,k}(2) = 25 p_k(0) \sum_{j=1}^{J-1} \sum_{j'=j+1}^{J} \frac{p_{\mathrm{d},jk}\, p_{\mathrm{d},j'k}}{\left(1-p_{\mathrm{d},jk}\right)\left(1-p_{\mathrm{d},j'k}\right)} . \tag{A32}$$

Finally, the field track-initiation probability $p_{\mathrm{ti,f}}$ is obtained from a combination of the track-initiation probabilities for each receiver:

$$p_{\mathrm{ti,f}} = 1 - \prod_{k=1}^{K} \left(1 - p_{\mathrm{ti},k}\right) . \tag{A33}$$

Multistatic, Centralised Tracking

In this case, $p_{\mathrm{ti,f}}$ is written as

$$p_{\mathrm{ti,f}} = 1 - p(0) - p(1) - p_1(2) - p_2(2) - p_3(2) - p_4(2), \tag{A34}$$

where $p(0)$ and $p(1)$ are the probabilities of exactly zero and one detection respectively in five pings of all sources, as before, $p_1(2)$ is the probability that a given source–receiver pair makes exactly two detections, $p_2(2)$ is the probability that the two detections involve the same source but different receivers, $p_3(2)$ the same receiver but different sources and, for $p_4(2)$, both sources and receivers are different for the two detections. The expressions for the probabilities are:

$$p(0) = \prod_{j=1}^{J} \prod_{k=1}^{K} \left(1 - p_{\mathrm{d},jk}\right)^5 , \tag{A35}$$

where $p_{\mathrm{d},jk}$ is the detection probability for the pair of source j and receiver k, which may or may not be collocated,

$$p(1) = 5p(0) \sum_{j=1}^{J} \sum_{k=1}^{K} \frac{p_{\mathrm{d},jk}}{1-p_{\mathrm{d},jk}} , \tag{A36}$$

$$p_1(2) = 10p(0) \sum_{j=1}^{J} \sum_{k=1}^{K} \left(\frac{p_{\mathrm{d},jk}}{1-p_{\mathrm{d},jk}} \right)^2 , \tag{A37}$$

$$p_2(2) = 25p(0) \sum_{j=1}^{J} \sum_{k=1}^{K-1} \sum_{k'=k+1}^{K} \frac{p_{\mathrm{d},jk}\, p_{\mathrm{d},jk'}}{\left(1-p_{\mathrm{d},jk}\right)\left(1-p_{\mathrm{d},jk'}\right)} , \tag{A38}$$

$$p_3(2) = 25p(0) \sum_{j=1}^{J-1} \sum_{j'=j+1}^{J} \sum_{k=1}^{K} \frac{p_{\mathrm{d},jk}\, p_{\mathrm{d},j'k}}{\left(1-p_{\mathrm{d},jk}\right)\left(1-p_{\mathrm{d},j'k}\right)} , \tag{A39}$$

and

$$p_4(2) = 25p(0) \sum_{j=1}^{J} \sum_{\substack{j'=1, \\ (j' \neq j)}}^{J} \sum_{k=1}^{K-1} \sum_{k'=k+1}^{K} \frac{p_{\mathrm{d},jk}\, p_{\mathrm{d},j'k'}}{\left(1-p_{\mathrm{d},jk}\right)\left(1-p_{\mathrm{d},j'k'}\right)} . \tag{A40}$$

In Equations (A36)–(A40), $p(0)$ refers to Equation (A35), not Equation (A24). For the field

layout used in this report, $p_2(2) = p_3(2)$ because sources and receivers are collocated, but this would not otherwise generally be the case.

A.3.2 Restriction to Five Pings

The track-initiation probability given by Equations (A22), (A23), (A28) or (A34), as the case may be, is the probability of starting a track after exactly 5 pings. Usually many more pings than this would be emitted during a tactical scenario. This can be handled analytically by a sliding-window approach, such as that discussed in §4.3 of reference 12 and used in the simulation described in reference 26. However, sliding-window methods are not appropriate for the present study because there is no natural upper limit to the number of pings that should be considered, and all probabilities approach 1.0 as the number of pings increases [12]. The impact of this limitation on the number of pings considered when computing the measure of performance is mitigated by the fact that the limitation applies equally to all cases.

Appendix B: Elaborations of the Method

B.1. Behaviour at Large Source–Receiver Separation

Section 2.2.1 illustrates a correction applied to the definition of R_{equiv} to overcome a problem with the behaviour of Equation (5) when the target is close to a receiver that is itself distant from the source. As discussed in §1.2.3, there are three candidates for the correction: a variation in the spreading law, near-field effects and absorption. The first two do not work, for the reasons given in §§B.1.3 and B.1.4 respectively. Subsections B.1.1 and B.1.2 detail the one that does work: absorption.

B.1.1 Correcting for Absorption

With the inclusion of absorption, Equations (3) and (4) for transmission loss become

$$\text{TL}_{\text{mono}} = 20 \log R^2 + 2\alpha R$$

$$\text{TL}_{\text{multi}} = 20 \log (R_{\text{ST}} R_{\text{TR}}) + \alpha(R_{\text{ST}} + R_{\text{TR}}), \tag{B1}$$

where α is the attenuation coefficient. It is clearly not possible to formulate a single definition of R_{equiv} that covers both the spreading and absorption terms simultaneously. We expect that, at acoustic frequencies typical of ASW sonar, spreading will dominate except at large distance, so we retain Equation (5) as the definition of R_{equiv} and apply a correction for absorption, using the so-called 'transition curve' [29(Fig.12.10)] to relate transmission loss and detection probability. The calculation involves the following steps:

- The uncorrected multistatic signal excess $\text{SE}_{\text{uncorr}}$ is computed from the uncorrected multistatic detection probability $p_{\text{d}}(R_{\text{equiv}})$ by

  $$\text{SE}_{\text{uncorr}} = \sigma_{\text{n}} \sqrt{2}\, \text{inv erf}\left(2 p_{\text{d}}\left(R_{\text{equiv}}\right) - 1\right), \tag{B2}$$

  where inv erf(·) is the inverse of the error function (eg. [45(ch.7)]) and σ_{n} is the standard deviation of the intensity of oceanic ambient noise. Following Urick [29], we take $\sigma_{\text{n}} = 8$ dB.
- Since transmission loss contributes linearly (in dB units) to signal excess, allowance for absorption amounts to a linear correction involving the difference in path lengths in the two lines of Equation (B1):

  $$\text{SE}_{\text{corr}} = \text{SE}_{\text{uncorr}} - \alpha\left(R_{\text{ST}} + R_{\text{TR}} - 2R_{\text{equiv}}\right). \tag{B3}$$

  The last term recognises that the monostatic p_{d} value includes a contribution from absorption, which means that the condition for the correction to be zero is stronger than $R_{\text{SR}} = 0$, it encompasses all situations where the target is equidistant from the source and receiver (i.e. $R_{\text{ST}} = R_{\text{TR}}$). The range difference—the term in brackets in

Equation (B3)—can never be negative (Appendix B.1.2); that is, $SE_{corr} \leq SE_{uncorr}$ always.

- Finally, the corrected signal excess is converted back to a detection probability:

$$p_{d,corr} = \frac{1}{2}\left[1 + \mathrm{erf}\left(\frac{SE_{corr}}{\sigma_n\sqrt{2}}\right)\right]. \tag{B4}$$

B.1.2 Notes on the Absorption Correction

Conversion to and from Signal Excess

The relationship between detection probability and signal excess (Eqns B2, B4) adopts the standard interpretation that SE = 0 is equivalent to $p_d = 0.5$, derived from the definition of signal excess as the amount by which the received signal level exceeds an operator-specified detection threshold. This is in accordance with the standard conception of a received signal as composed of a deterministic part arising from acoustic scattering from external objects and a randomly fluctuating component arising from ambient oceanic noise [35]. Then, given the reasonable assumption that the random fluctuations are symmetric about their mean, one expects that, when the average signal level exactly equals the detection threshold, the total signal will exceed the threshold for half the time and fall below it for the other half. Hence $p_d = 0.5$.

Obtaining SE values at p_d values away from 0.5 requires further assumptions on the nature of the oceanic noise fluctuations. Equations (B2) and (B4) assume Gaussian noise with standard deviation of σ_n. There is less empirical support for this assumption than for symmetry about the mean. However, as elsewhere, we rely on the relative nature of the analysis: the assumptions impact the results only to the extent that they affect the monostatic and multistatic geometries differently.

Correction to Signal Excess is never Positive

We seek to demonstrate that, in Equation (B3), SE_{corr} is not greater than SE_{uncorr}, irrespective of the geometry. It amounts to showing that

$$D = R_{ST} + R_{TR} - 2R_{equiv} \geq 0 \tag{5}$$

always. Define the following quantities:

$$\bar{R} = \tfrac{1}{2}\left(R_{ST} + R_{TR}\right), \quad \Delta = \tfrac{1}{2}\left|R_{ST} - R_{TR}\right|. \tag{6}$$

Then, because of its symmetry, the expression for D is

$$D = 2\bar{R} - 2\bar{R}\sqrt{(1-\Delta)(1+\Delta)}, \tag{7}$$

regardless of which of R_{ST} or R_{TR} is the larger. Hence

$$D = 2\bar{R}\left(1 - \sqrt{1-\Delta^2}\right), \tag{8}$$

which is not less than zero for any value of Δ. This is hardly surprising, for the analysis above merely rehearses the proof that the geometric mean of two real numbers is never larger than their arithmetic mean—a very well known result (e.g. [46(p.504)]).

When p_d *Equals 1.0*

Equation (B2) gives $SE_{uncorr} = \infty$ when $p_d = 1.0$. It means that the correction procedure does not work with an ideal definite-range p_d curve. Here is another reason for going beyond the cookie cutter for modelling multistatics.

B.1.3 Variation in the Spreading Law

Equation (5) is based on spherical spreading, which assumes a uniform ocean in all directions. All environments, however, are limited in vertical extent, by the surface and by either the bottom or the maximum depth of acoustic rays in upwardly refracting conditions. The effect of this on spreading loss is usually modelled as spherical spreading out to a 'transition range' R_c, beyond which the spreading is cylindrical [29(p.152),47]. That is, Equation (3) becomes

$$TL_{mono} = \begin{cases} 40\log R & \text{if } R \le R_c \\ 20\log(R_c R) & \text{if } R > R_c \end{cases} \tag{B9}$$

and its multistatic equivalent, Equation (4), becomes

$$TL_{multi} = \begin{cases} 20\log(R_{ST} R_{TR}) & \text{if } R_{ST} \le R_c \text{ and } R_{TR} \le R_c \\ 10\log\left(R_{ST} {R_{TR}}^2 R_c\right) & \text{if } R_{ST} > R_c \text{ and } R_{TR} \le R_c \\ 10\log\left({R_{ST}}^2 R_{TR} R_c\right) & \text{if } R_{ST} \le R_c \text{ and } R_{TR} > R_c \\ 10\log\left(R_{ST} R_{TR} {R_c}^2\right) & \text{if } R_{ST} > R_c \text{ and } R_{TR} > R_c. \end{cases} \tag{B10}$$

It is immediately clear that cylindrical spreading cannot provide a solution to the difficulties with Equation (5); for all the lines in Equation (B10) involve the product of R_{ST} and R_{TR}, so all exhibit the same undesirable behaviour as Equation (5). Nevertheless, we added Equation (B10) to the MATLAB code to check its effect, by adapting the procedure of Appendix B.1.1. In summary:

- Compute multistatic p_d using Equation (5) and the monostatic p_d curve of choice.
- Convert to uncorrected signal excess using Equation (B2).
- Apply the correction as the difference between Equations (B9) and (B10).
- Convert back to p_d using Equation (B4).

Results are shown in Figure B1 for the somewhat extreme case of a large source–receiver distance—$9R_0$—and a small transition range: just R_0. Despite this effort to magnify the effect, it remains modest, as indicated by dotted line.

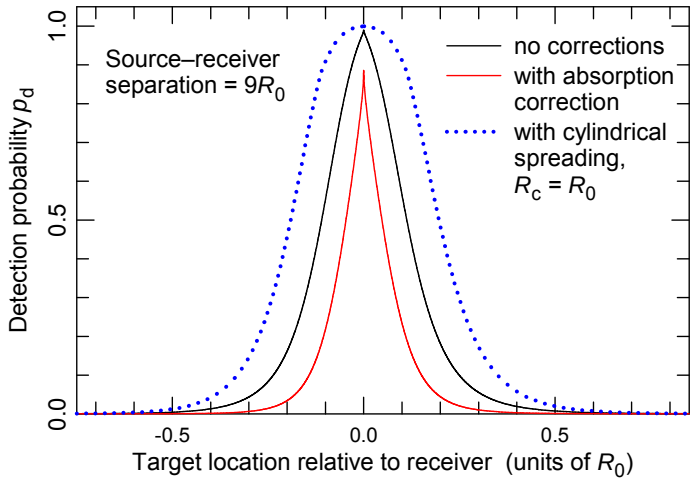

Figure B1: As in Figure 6, but with a dotted blue line showing the effect of cylindrical spreading assuming $R_c = R_0$ *(and no absorption correction)*

Note also that this correction goes in the opposite direction to the correction for absorption; that is, it increases coverage area. This is to be expected; for, with cylindrical spreading, signal level decreases more slowly as range increases than with spherical spreading.

B.1.4 Near-Field Effects

Expressions such as Equations (3), (4), (B9) and (B10) are accurate only beyond a certain distance from a scatterer, in what is known as the 'far field'. Far-field conditions involve:

- the range,
- the wavelength λ of the acoustic wave,
- the shape of the scatterer (i.e. sphere, cylinder, etc.), and
- the dimensions and orientation of the scatterer.

The condition on wavelength is $\lambda < 2\pi a$, where a is a 'typical' dimension of the scatterer [29(p.303)]. At a frequency of 2 kHz, the acoustic wavelength in water is about 0.8 m, and smaller at higher frequencies, hence submarine-sized objects fulfil this condition.

The condition involving range depends on the shape and orientation of the scatterer. For a sphere, one requires $R > a$, where a is the radius of the sphere [29(p.303)]. This also applies to a part of a sphere. So, for example, the bow section of a submarine may be piecewise spherical with a radius of several metre. Then far-field conditions apply that same number of metres from the bow. In other words, when viewing the submarine bow-on, the near-field region is negligibly small, from the point of view of ASW operations.

On the other hand, the far-field condition perpendicular to the axis of a cylinder of length L and radius a is $R > L^2/\lambda$ (and also $\lambda < 2\pi a$, as above). For a length of 80 m and $\lambda = 0.8$ m (i.e. an acoustic frequency of 2 kHz), this evaluates to $R > 8$ km, indicating that near-field effects may be present at tactically interesting ranges when beam on to a submarine.

The near field can be thought of as a region of overlapping wavelets that spread spherically from every point on the surface of the scatterer. It means that the acoustic field may display interference minima and maxima, the amplitude and locations of which cannot be determined simply. The most that simple arguments can give are the expectations that the amplitude should diminish with increasing distance from the scatterer, to be negligible at the range given by the far-field condition, and that interference features should be spaced about λ apart, which is of order meters. This spacing makes it difficult to fall back on our usual argument that, because the effect applies equally to monostatics as multistatics, it ought to largely cancel; for moving a receiver by a distance only of order λ may change the detection probability, perhaps markedly, depending on the interference amplitude in the region in question. However, this picture also suggests that near-field effects are (approximately) periodic, which means that they (approximately) average out over distances of order many λ, which in turn would suggest that they ought not to have a large impact on a total coverage area. Real contours in plots like Figure 11 may be less regular than shown, leading to small (dimensions less than or of order λ) undetected coverage gaps, but the effects probably wash out when averaged over regions of dimension much larger than λ, and would in any case be broadly similar for monostatics and multistatics. Hence we expect any effects on the final comparative results to be small.

However much the above argument may seem unsatisfactory (because unquantitative), it is the best currently available, to our knowledge, short of a full coherent wavelet summation, and that would take the calculations to a level of complexity scarcely compatible with the aspirations of operations analysis.

B.2. Bearing-Dependent and Realistic Detection Probabilities

The monostatic detection-probability models used in this report—Equations (1), (6) and (7)—are schematic. It is clearly straightforward to extend the method to realistic p_d curves, such as those from acoustic-propagation modelling (e.g. [12(§4.6)]). This may provide a method of approximating a full multistatic acoustic-propagation calculation, which can be very time-consuming. However, the degree of accuracy achievable is yet to be explored and is probably environment-dependent.

Equations (1), (6) and (7) are also independent of the bearing of the target from the sensor. This is appropriate for sonobuoys and dipping sonars, but towed line arrays, for example, show lower p_d at end-fire than broadside. It is clearly not difficult to extend the analysis to bearing-dependent sensors. The coverage-area results would then depend on the relative orientation of neighbouring sensors as well as the spacing between them. An example for a small field of monostatic sensors is shown in Figure 33 of reference 12.

B.3. Aspect-Dependent Target Strength

The possibility of 'glint' (i.e. specular) reflections from a target is one of the attractions of multistatics, and there are analyses of how to lay out a field to maximise it (e.g. [22]). Glint reflections can occur with monostatic sensors, of course, but submarine COs are careful to

avoid them, which they can do because they know the bearing of each active sensor within range. When facing a multistatic field, on the other hand, the submariner knows only the locations of the sources.

The method of correcting for absorption provides a template for the inclusion of aspect-dependent target strength: having converted p_d to signal excess, a correction for bistatic target strength can be applied. In general, bistatic target strength is a function of two angles, the bistatic angle φ and the bistatic aspect angle α, as defined in Figure 2 (p. 4). The so-called 'bistatic theorem' (e.g. [48]) states that target strength is a function of α only, but this is an approximation, as Cox explains [15].

Inclusion of aspect-dependent target strength means that, on a coverage-area plot, the probability becomes a function of α. Hence, some assumption about submarine location and heading is required. The results do not explicitly depend on φ, regardless of whether the bistatic theorem is adopted, because φ has a unique value at each point on a coverage-area plot. That is, such φ dependence as may exist and as the analyst chooses to include is automatically accounted for in the coverage calculations.

Appendix C: Matlab Code

This appendix contains listings of two Matlab codes used to compute the multistatic coverage-area diagrams in the body of this report. The first, giving p_d for a bistatic pair including both the absorption and cylindrical spreading-loss corrections, produced Figures 3, 5–8 and B1. The second, giving field track-initiation probability for a field of collocated source–receiver pairs, includes only the absorption correction. It produced Figures 11–15 and the results in Figures 16 and 17.

C.1. Bistatic Pair

```
% Plotting & display code for the bistatic case when transmission loss is dealt with properly for
% absorption AND spreading, showing contours of DETECTION PROBABILITY (not pti).
%
clear all
%  ---------- Data entry ---------------
%
% Set the vector of source--receiver separations; the code generates one plot for each
% separation.  A monostatic calculation results when Rsr is zero. Rsr is a fraction of r0.

Rsr = [0 1 2 3 4 5 6 7];

% set the type of the equivalent monostatic pd profile

%ptype = 'cookie';
%ptype = 'exp';
ptype = 'Fermi';

% set parameters of pd-profile functions (the third is used by Fermi only)

p0 = 1.0;      % peak pd
r0 = 10.0;     % characteristic range in km
b = 0.5;       % diffusivity (fraction of r0) for Fermi function

% Set the pulse length Rp and multistatic signal-processing pulse-compression factor pcf.
% The target is in the blind zone if Rst + Rrt < Rsr + Rp/pcf (multistatics) or R < Rp/2 (monostatics).
% (Rrt --- receiver--target distance, Rst --- source--target distance.)

Rp = 0;    % in km; set to zero to switch blast-zone checking off.
pcf = 1;   % must be greater than or equal to 1 (= 1 for no compression)

% Set attentuation coefficient to be used in the absorption correction & noise standard deviation

attenuation = 0.0;   % dB/km; set to zero to switch correction off
noise_sd = 8.0;      % dB

% Set whether to include cylindrical spreading transmission loss. TL = 'spreading' means
% include. Set Rc, the range at which to switch to cylindrical spreading.
```

```
 %TL = 'no correction';
TL = 'spreading';
Rc = 10;              % km

% Set the scale for the contour plots (in km).  (The first line is the default; switch to the
% second line for explicit control of the scale.)

plot_scale = max(r0*Rsr);
%plot_scale = 50;

% ------------ End data entry -------------


% Set up grid of target locations. Receiver is located at the origin, source is on the x axis at
% location +Rsr(i).  However, all i contour plots have the same plot limits, determined by the
% largest of the Rsr values (or the nominated value).

if strcmp('exp', ptype)
   range_of_the_day = r0 * log10(2*p0);
   around = range_of_the_day * 1.5 ;
elseif strcmp('Fermi', ptype)
   range_of_the_day = r0*(1 + (1/b)*log10(2*p0 - 1));
   around = range_of_the_day * 2.3;
else
   range_of_the_day = r0;
   around = range_of_the_day * 1.05;
end
meshstep = (plot_scale + around*1.7)/1000;
targx = -around:meshstep:plot_scale + around*0.7;
targy = -around:meshstep:around;
[gridx,gridy] = meshgrid(targx,targy);

% Calculate receiver--target distances
Rrt = sqrt(gridx.^2 + gridy.^2);

% Determine number of source--receiver distances to plot; set contour levels; set up the line
% plots, including constructing the title & labelling the axes

Rsr_len = size(r0*Rsr);
nplot = Rsr_len(2);
contourlevels = 0.0:0.01:1.0;
line_plot = figure; orient tall
subplot(2,1,1); hold on
plot_title = {'\fontsize{11}Bistatic {\itp}_d  (incl. absorption & cylindrical spreading)'; ...
              ['Range of the day = ' num2str(range_of_the_day,%11.2g') ' km_ ']; ...
              ['\fontsize{9}Pulse length for blast zone = ' num2str(Rp) ...
               ' km,_  pulse compression factor = ' num2str(pcf)]; ...
               '4th line'; '5th line'; '  '; '\fontsize{10}Transect along receiver--source line'};
if strcmp('spreading', TL)
   plot_title{4} = ['attenuation coeff = ' num2str(attenuation) ' dB/km,_  noise std dev = ' ...
                    num2str(noise_sd) ' dB,  transition radius = ' num2str(Rc) ' km'];
else
   plot_title{4} = ['attenuation coeff = ' num2str(attenuation) ' dB/km,_  noise std dev = ' ...
                    num2str(noise_sd) ' dB'];
end
```

```
if strcmp('exp', ptype)
   plot_title{5} = ['Equivalent monostatic {\itp}_d:  exponential,  {\itp}_0 = ' num2str(p0) ...
                    ',  {\itr}_0 = ' num2str(r0) 'km'];
elseif strcmp('Fermi', ptype)
   plot_title{5} = ['Equivalent monostatic {\itp}_d:  Fermi,  {\itp}_0 =  ' num2str(p0) ...
                    ',  {\itr}_0 = ' num2str(r0) ' km,  diffusivity = ' num2str(b)];
else
   plot_title{5} = ['Equivalent monostatic {\itp}_d:  cookie-cutter,  {\itp}_0 = ' ...
                    num2str(p0) ',  {\itr}_0 = ' num2str(r0) ' km'];
end

title(plot_title)
axis ([min(targx), max(targx), 0., 1.0])
xlabel('Distance  (km)'); ylabel('{\itp}_d')
x_ind = find((targy + meshstep/2) >= 0, 1);
y_ind = find((targx + meshstep/2) >= 0, 1);
subplot(2,1,2); hold on
title('Transect perpendicular to receiver--source line at location of receiver')
axis ([min(targy), max(targy), 0, 1.0])
xlabel('Distance  (km)'); ylabel('{\itp}_d')
lineC = line_colour;

% For each source--receiver distance ...
for i = 1:nplot
   % compute the Rst values and equivalent monostatic distances
   Rst = sqrt((gridx - r0*Rsr(i)).^2 + gridy.^2);
   Requiv = sqrt(Rst.*Rrt);

   % compute the pd values (ignoring the blast zone to begin with)
   if strcmp('exp', ptype)
      pd = p0 * 10.^(-Requiv/r0);
   elseif strcmp('Fermi', ptype)
      pd = p0 * (1 + 10.^((Requiv/r0 - 1)/b)).^(-1);
   else
      pd =(Requiv <= r0);
      pd = p0 * pd;
   end

   % set up for corrections --- compute the signal excess from pd
   se = (sqrt(2)* noise_sd) .* erfinv(2.*pd - 1);
   % apply the absorption correction
   se = se - attenuation .* (Rst + Rrt - 2*Requiv);
   % check whether to apply correction for cylindrical spreading
   if strcmp('spreading',TL)
      % Case 1 --- Rrt > Rc, Rst <= Rc; compute the cylindrical transmission loss
      % minus the spherical transmission loss
      spreading_1 = -20.*log10(Rst) - 10.*log10(Rrt.*Rc);
      % Case 2 --- Rst > Rc, Rrt <= Rc; ditto
      spreading_2 = -20.*log10(Rrt) - 10.*log10(Rst.*Rc);
      % Calculate regions for which we assume equivalent monostatic is in
      % cylindrical and spherical phases and add on the appropriate monostatic
      % transmission loss.
      sphere = (Requiv <= Rc);
      cylinder = (Requiv > Rc);
      spreading_1(sphere) = spreading_1(sphere) + 40.*log10(Requiv(sphere));
      spreading_1(cylinder) = spreading_1(cylinder) + 20.*log10(Requiv(cylinder)*Rc);
```

```
        spreading_2(sphere) = spreading_2(sphere) + 40.*log10(Requiv(sphere));
        spreading_2(cylinder) = spreading_2(cylinder) + 20.*log10(Requiv(cylinder)*Rc);
        % Calculate regions for which spreading_1 and spreading_2 do not occur.
        outer_1 = (Rrt <= Rc | Rst > Rc);
        spreading_1(outer_1) = 0;
        outer_2 = (Rst <= Rc | Rrt > Rc);
        spreading_2(outer_2) = 0;
        % Apply correction
        spreading = spreading_1 + spreading_2;
        se = se + spreading;
    end

    % Recalculate pd from signal excess
    pd = 0.5*(1 + erf(se ./ (sqrt(2) * noise_sd)));

    % Blind zone --- set up the logical mask indicating which target locations are inside the blind
    % zone & use it to zero out that part of the pd array.  Note that the pulse-compression factor
    % does not apply for the monostatic configuration. (Actually, set pd values to -0.1 inside the
    % blind zone so that blind-zone delineation works properly in the plots.)

    Rb = Rp;
    if (Rsr(i) > 0)
        Rb = Rp/pcf;
    end
    blast = (Rst + Rrt < r0*Rsr(i) + Rb);
    pd(blast) = -0.1;

    % add lines to the 2-d plot
    figure(line_plot)
    subplot(2,1,1)
    % plot pd along (or near to) the x axis
    plot(targx, pd(x_ind,:), 'LineStyle', '-', 'Color', lineC(i,:))
    subplot(2,1,2)
    % plot pd along (or near to) the y axis, i.e. receiver location
    plot(targy, pd(:,y_ind), 'LineStyle', '-', 'Color', lineC(i,:))

    % Set up for the contour plot.
    figure; orient landscape; hold on
    axis equal; axis ([min(targx), max(targx), min(targy), max(targy)]);
    h = gca; set (h, 'TickLength', [0.05, 0.1]);
    xlabel('Distance  (km)'); ylabel('Distance  (km)')
    caxis([0.0 1.0]); colormap(pdmapMPF); colorbar('EastOutside')
    % Adapt the title and apply ...
    plot_title{6} = '\fontsize{6}  ';
    plot_title{7} = ['\fontsize{11}_ Source -- receiver distance = ' ...
                num2str(r0*Rsr(i)) ' km_ '];
    title(plot_title)

    % Produce a filled contour plot, then overlay with a thin contour line around the blind zone.
    % Plot markers at the locations of the source and receiver.

    contourf(gridx, gridy, pd, contourlevels, 'LineStyle', 'none')
    contour (gridx, gridy, pd, [-0.1 -0.1], '-k', 'LineWidth', 0.2)
    plot(r0*Rsr(i), 0, 'kp', 'MarkerFaceColor', 'k', 'MarkerSize', 40)
    plot(0, 0, 'ko', 'MarkerFaceColor', 'k', 'MarkerSize', 27)
    hold off
end
```

C.2. Field of Collocated Sources and Receivers

```
% Plotting & display code for the case of many collocated source-receiver pairs.
% Can be run distributed monostatic, networked monostatic, distributed multistatic or networked
% multistatic.   Metric is probability of track initiation using 3-in-5.
clear all

%  ---------- Data entry ----------

% Set parameters of pd-profile functions. (The third is used by Fermi only.)
p0 = 1.0;          % peak pd
r0 = 10.0;         % characteristic range
b = 0.5;           % (r_0.1 - r_0.5) / r0*log10((10*p0 - 1) / (2p0 - 1)) ... fraction of range of day

% Set a vector of sonar spacing values. (One plot is produced for each value in such
% a way that all plots have the same scale.)  Then set the array of source--receiver
% locations as a fraction of that spacing value.
% (One row --- x val, y val --- for each sonar in the field.)
%area = [60];

spacing = [8.2   8.3   8.4];
pattern = [0         0; ...
         0.0       1.0;      0.0      -1.0; ...
         0.86603   0.5;      0.86603  -0.5; ...
        -0.86603   0.5;     -0.86603  -0.5; ...
         0.86603   1.5;      0.86603  -1.5; ...
        -0.86603   1.5;     -0.86603  -1.5; ...

         1.73205   0.0;     -1.73205   0.0; ...
         1.73205   1.0;      1.73205  -1.0; ...
        -1.73205   1.0;     -1.73205  -1.0; ...
         0.0       2.0;      0.0      -2.0
         ];

% Choose one of the following 4 lines to set the mode of operation of the sonar field.
%mode = 'Monostatic with distributed tracking';
%mode = 'Monostatic with networked tracking';
%mode = 'Multistatic with distributed tracking';
mode = 'Multistatic with networked tracking';

% Choose one to set the type of the equivalent monostatic pd profile.

ptype = 'exp';
%ptype = 'Fermi';

% Set the blast-zone length Rb and multistatic pulse-compression factor pcf.  The target is in
% the blast zone if R < Rb/2 for monostatics or Rst + Rrt < Rsr + Rb/pcf for multistatics.
% (R = monostatic range, Rst = source--target distance, Rrt = receiver--target distance,
% Rsr = source--receiver distance.)

Rb = 1.5;        % Distance units; set to zero to switch blast-zone checking off.
pcf = 1;         % Must be >= 1; set to 1 to turn pulse compression off.

% Set the scale for the plot (in distance units).  (The first line is the default;
% switch to the second line for explicit control of the scale.)
```

```
plot_scale = max(r0*spacing);
%plot_scale = 20;
%absorption = 'off';
absorption = 'on';

%Set attenuation (dB/km) to be used in absorption.
attenuation = 0.1;
%Set noise standard deviation (dB) to be used in absorption.
noise_sd = 8;

 % ------------ End of data entry --------------
%
%
% Set up grid of target locations.
meshstep = plot_scale/50;
max_vals = max(pattern) * plot_scale;
min_vals = min(pattern) * plot_scale;
if strcmp('exp', ptype)
   range_of_the_day = r0;
   around = range_of_the_day  * 3;
else
   range_of_the_day = r0+(r0/b)*log10(2*p0 - 1);
   around = range_of_the_day * 1.5;
end
targx = (min_vals(1) - around):meshstep:(max_vals(1) + around);
targy = (min_vals(2) - around):meshstep:(max_vals(2) + around);
[gridx,gridy] = meshgrid(targx,targy);

% Determine number of field spacings to compute & number of sonars in the field;
% set the levels for the filled contour plots.
sp_len = size(r0*spacing);
ncases = sp_len(2);
snr_len = size(pattern);
nsnrs = snr_len(1);
contourlevels = 0.0:0.01:1.0;

for icase = 1:ncases

   %Initialise ratio of detection store. Each cell(source, receiver) of r_d_store contains the r_d
   % values for that particular source and receiver. Within each cell is a gridx,gridy matrix.
   r_d_store = cell(nsnrs,nsnrs);
   %initialise matrix for prob of getting zero detections at all receivers after each source has
   % pinged 5 times — multistatics
   pr0 = ones(size(gridx));
   %initialise matrix for getting zero detections at all receivers after their respective sources
   % have pinged 5 times — monostatics
   pr0_mono = ones(size(gridx));
   %initialise pti field
   pti_field = ones(size(gridx));
   %The above must reset for each of the ncases
   % Calculate sonar locations.
   sonars = pattern * r0 * spacing(icase);

   for ircvr = 1:nsnrs
      % Compute the array of source--target distances.
      Rrt = sqrt((gridx - sonars(ircvr,1)).^2 + (gridy - sonars(ircvr,2)).^2);
```

```
%initialise matrix for probability of 0 detections at k after 5 pings from each source
%Must reset for each sonar as receiver
pr0_k = ones(size(gridx));

if strcmp('Monostatic with distributed tracking', mode) || ...
                                        strcmp('Monostatic with networked tracking', mode)

   %calculate equivalent multistatic range (not incl TLabsorption - only TLspreading)
   Requiv = sqrt((gridx - sonars(ircvr,1)).^2 + (gridy - sonars(ircvr,2)).^2);

   % Compute the pd values, ignoring the blast zone.
   if strcmp('exp', ptype)
      pd = p0 * 10.^(-log10(2)*Requiv/r0);
   else
      pd = p0 * (1 + 10.^(((Requiv/r0) - 1)/b)).^(-1);
   end
   % Compute & apply the mask to zero out probabilities in the blast zone.
   blast = (Requiv < Rb/2);
   pd(blast) = 0.;

   if strcmp('Monostatic with distributed tracking', mode)
      %Calculate individual pti for sonobuoy then increment pti_field
      pti = pd.^3 .* (10 - 15*pd + 6*pd.^2);
      pti_field = pti_field .* (1 - pti);
   end

   %increment probability of no detections from any sonobuoy
   pr0_mono = pr0_mono.*(1-pd).^5;
   %calculate ratio of detection to no detection and store each receivers.
   r_d = pd ./ (1 - pd);
   r_d_store(ircvr, ircvr) = {r_d};

else
   for isrce = 1:nsnrs

      % Compute the source--receiver, receiver--target and equivalent monostatic
      % distances (N.B. the monostatic case in INCLUDED; i.e. a sonar can act both as
      % source and receiver.)
      Rsr = sqrt((sonars(isrce,1) - sonars(ircvr,1))^2 + ...
                                                (sonars(isrce,2) - sonars(ircvr,2))^2);
      Rst = sqrt((gridx - sonars(isrce, 1)).^2 + (gridy - sonars(isrce,2)).^2);
      Requiv = sqrt(Rst.*Rrt);
       % Compute the pd values, ignoring the blast zone.
      if strcmp('exp', ptype)
         pd = p0 * 10.^(-log10(2)*Requiv/r0);
      else
         pd = p0 * (1 + 10.^(((Requiv/r0) - 1)/b)).^(-1);
      end

      if strcmp('on', absorption)
         %compute the signal excess for pd
         se = sqrt(2)*noise_sd .* erfinv(2.*pd - 1);
         %add in the absorption term
         se = se - attenuation.*(Rst + Rrt) + 2*attenuation*Requiv;
         %recalculate pd from signal excess
         pd = 0.5*(1 + erf(se ./ (sqrt(2)*noise_sd)));
      end
```

```
            % Compute & apply mask to zero out probabilities in the blast zone.
            blast = (Rst + Rrt < Rsr + Rb/pcf);
            pd(blast) = 0.;
            %increment pr0_k - probability of no detections at receiver k from any source after
            %each has pinged five times.
            pr0_k = pr0_k.*(1 - pd).^5;
            %ratio of detection to no detection.
            r_d = pd ./ (1 - pd);
            r_d_store(ircvr, isrce) = {r_d};
        end
    end

    %increment pr0 - the probability of no detections at any receiver after each source has
    % pinged 5 times.
    pr0 = pr0.*pr0_k;

    %This is where the multi dist stuff belongs - calculate the pti for each receiver:
    if strcmp('Multistatic with distributed tracking', mode)
        %start tracks at
        r_d_1 = zeros(size(gridx));
        r_d_2_1 = zeros(size(gridx));
        r_d_2_2 = zeros(size(gridx));
        %rd calculation
        for u = 1:nsnrs
            r_d_1 = r_d_1 + r_d_store{u,ircvr}(:,:);
            r_d_2_1 = r_d_2_1 + (r_d_store{u,ircvr}(:,:)).^2;
        end
        %Calculate probability of one detection
        pr1 = 5*r_d_1.*pr0_k;
        %calculation for probability exactly 2 (1). 10 is from 5C2.
        pr2_1 = 10*r_d_2_1.*pr0_k;
        %calculation for probability exactly 2 (2). 25 is from (5C1)^2.
        for u = 1:nsnrs-1
            for w = u+1:nsnrs
                r_d_2_2 = r_d_2_2 + r_d_store{u,ircvr}(:,:).*r_d_store{w,ircvr}(:,:);
            end
        end
        pr2_2 = 25*r_d_2_2.*pr0_k;
        pr2 = pr2_1 + pr2_2;

        pti = 1 - pr0_k - pr1 - pr2;
        pti_field = pti_field.*(1-pti);
    end
end

if strcmp('Multistatic with distributed tracking', mode) || ...
                                        strcmp('Monostatic with distributed tracking', mode)
    pti_field = 1-pti_field;
end

%For the netowrked multistatic case
if strcmp('Multistatic with networked tracking', mode)
    r_d_1 = zeros(size(gridx));
    r_d_2_1 = zeros(size(gridx));
    r_d_2_2 = zeros(size(gridx));
    r_d_2_3 = zeros(size(gridx));
```

```
    %rd calculation for probability of detecting exactly one and
    %exactly two from one pair
    for u = 1:nsnrs
        for v = 1:nsnrs
            r_d_1 = r_d_1 + r_d_store{u,v}(:,:);
            r_d_2_1 = r_d_2_1 + (r_d_store{u,v}(:,:)).^2;
        end
        for v = 1:nsnrs-1
            for w = v+1:nsnrs
                r_d_2_2 = r_d_2_2 + r_d_store{u,v}(:,:).*r_d_store{u,w}(:,:);
                for x = 1:nsnrs
                    if x~=u
                        r_d_2_3 = r_d_2_3 + r_d_store{u,v}(:,:).*r_d_store{x,w}(:,:);
                    end
                end
            end
        end
    end

    %Calculate probability of one detection
    pr1 = 5*r_d_1.*pr0;
    %Calculate probability of 2 detections from same source and
    %receiver
    pr2_1 = 10*r_d_2_1;
    %calculation for probability exactly 2 (2). 25 is from (5C1)^2.
    pr2_2 = 25*r_d_2_2;
    %calculation for probability exactly 2 (3). 25 is from (5C1)^2.
    pr2_3 = 25*r_d_2_3;

    pr2 = pr0.*(pr2_1 + pr2_2 + pr2_3);

    pti_field = 1 - pr0 - pr1 - pr2;
end
if strcmp('Monostatic with networked tracking', mode)
    r_d_1 = zeros(size(gridx));
    r_d_2_1 = zeros(size(gridx));
    r_d_2_2 = zeros(size(gridx));
    for u = 1:nsnrs
        r_d_1 = r_d_1 + r_d_store{u,u}(:,:);
        r_d_2_1 = r_d_2_1 + (r_d_store{u,u}(:,:)).^2;
    end
    for u = 1:nsnrs-1
        for v = u+1:nsnrs
            r_d_2_2 = r_d_2_2 + r_d_store{u,u}(:,:).*r_d_store{v,v}(:,:);
        end
    end
    pr1 = 5*r_d_1.*pr0_mono;
    pr2 = (10*r_d_2_1 + 25*r_d_2_2).*pr0_mono;

    pti_field = 1 - pr0_mono - pr1 - pr2;
end

    % Set up to plot the field pti.
    figure ('PaperType', 'A3'); orient tall; hold on
    axis equal; axis ([min(targx), max(targx), min(targy), max(targy)])
    xlabel ('Distance  (km)'); ylabel ('Distance  (km)')
    caxis([0 1.0]); colormap(pdmapMPF); colorbar('EastOutside')
```

```
        % Construct and apply the appropriate title ...
        plot_title = {'\fontsize{12} Collocated sources & receivers _ '; '2nd line'; ...
                      ' Contours of {\itp}_t_i using 3-in-5 track initiation'; ...
                     ['\fontsize{10}_ Pulse length for blast zone = ' num2str(Rb) ...
                     ' km,  pulse compression factor = ' num2str(pcf)]; '5th line'; ...
                     '\fontsize{3} '; ['\fontsize{12} Sonar separation = ' ...
                    num2str(r0 * spacing(icase)) ' km,  Range of the day ({\itR}_0)= ' ...
                    num2str(range_of_the_day, '%11.2g') ' km_ ']; ...
                    ['Absorption = ' num2str(absorption)]};
        plot_title{2} = num2str(mode);
        plot_title{5} = ['Equivalent monostatic {\itp}_d:'  num2str(ptype) ',  {\itp}' ...
                         '_0 = ' num2str(p0) ',  diffusivity = ' num2str(b)];
        title(plot_title)

        % Produce a filled contour plot, then overlay with a thick contour line at the 0.5 level and
        % draw markers at the location of each sonar
        contourf(gridx, gridy, pti_field, contourlevels, 'LineStyle', 'none')
        contour (gridx, gridy, pti_field, [0.5 0.5], '-k', 'LineWidth', 1.2)
        for isnr = 1:nsnrs
           plot(sonars(isnr,1), sonars(isnr,2), 'ko', 'MarkerFaceColor', 'k', 'MarkerSize', 4)
        end
        hold off
    end
```

References

[1] W.J.R. Gardner (1996) *Anti-submarine warfare*, Brassey's, London.

[2] D. Stevens (2005) *A critical vulnerability—the impact of the submarine threat on Australia's maritime defence 1915–1954*, Royal Australian Navy Sea-Power Centre—Australia, Papers in Australian Maritime Affairs, no. 15.

[3] A. Davies (2007) 'The enemy below: Anti-submarine warfare in the ADF', special report no. 2 of the Australian Strategic Policy Institute.

[4] A. Davies (2008) 'ADF capability review: Royal Australian Navy', policy analysis paper 23 of the Australian Strategic Policy Institute.

[5] A. Davies (2009) 'Australian naval combat helocopters—the future', special report no. 21 of the Australian Strategic Policy Institute.

[6] S. Zimmerman (1997) *Submarine technology for the 21st century*, Pasha Publications, Arlington VA.

[7] J.I. Bowen & R.W. Mitnick (1999) 'A multistatic performance prediction methodology', *Johns Hopkins APL Technical Digest*, vol. 20, pp. 424–31.

[8] M.P. Fewell (2008) 'Developments in submarine capability relevant to anti-submarine warfare by fixed-wing aircraft', general document DSTO-GD-0545 of the Defence Science and Technology Organisation, CLASSIFIED.

[9] CMDR M. Hammond (2006) *An effects-based anti-submarine warfare strategy*, Royal Australian Navy Sea-Power Centre—Australia, Working Paper 19.

[10] M.J. Walsh & T.A. Wettergren (2008) 'Search performance prediction for multistatic sensor fields', *Proceedings IEEE Oceans 2008*.

[11] D. Grimmett & S. Coraluppi (2006) 'Contact-level multistatic sonar data simulator for tracker performance assessment', *Proceedings 9th International Conference on Information Fusion*, Florence.

[12] M.P. Fewell, J.M. Thredgold & D.J. Kershaw (2008) 'Benefits of sharing detections for networked track initiation in anti-submarine warfare', technical report DSTO-TR-2086 of the Defence Science and Technology Organisation.

[13] J.M. Thredgold & M.P. Fewell (2010) 'Distributed versus centralised tracking in networked anti-submarine warfare', technical report DSTO-TR-2373 of the Defence Science and Technology Organisation.

[14] J.M. Thredgold, M.P. Fewell, S.J. Lourey & H.X. Vu (2010) 'Performance assessment of sonar-system networks for anti-submarine warfare', *Proceedings IEEE OCEANS '10*, Sydney.

[15] H. Cox (1989) 'Fundamentals of bistatic active sonar' in Y.T. Chan (ed.) *Underwater acoustic data processing*, Kluwer Academic, pp. 3–24.

[16] D. Grimmett & S. Coraluppi (2004) 'Sensitivity analysis for multistatic LFAS localisation accuracy', report SR-386 of the NATO Undersea Research Centre.

[17] S. Coraluppi & C. Carthel (2005) 'Distibuted tracking in Multistatic Sonar', *IEEE Transactions on Aerospace and Electronic Systems*, vol. 41, p. 1138–47.

[18] S. Coraluppi, D. Grimmett & P. de Theije (2006) 'Benchmark evaluation of multistatic trackers', report NURC-PR-2006-007 of the NATO Undersea Research Centre.

[19] B.I. Incze & S.B. Dasinger (2006) 'A Bayesian method for managing uncertainties relating to distributed multistatic sensor search', *Proceedings 9th International Conference on Information Fusion*, Florence.

[20] D. Grimmett (2006) 'Multi-sensor placement to exploit complementary properties of diverse sonar waveforms', *Proceedings 9th International Conference on Information Fusion*, Florence.

[21] T. Lang & G. Hayes (2007) 'Evaluation of an MHT-enabled tracker with simulated multistatic sonar data', *Proceedings IEEE Oceans 2007 – Europe*.

[22] D.J. Grimmett, S. Sullivan & J. Alsup (2008) 'Modeling specular occurrence in distributed multistatic fields', *Proceedings IEEE Oceans 2008 – MTS/IEEE Kobe Techno-Ocean*.

[23] F. Ehlers, M. Daun & M. Ulmke (2009) 'System design and fusion techniques for multistatic active sonar', *Proceedings IEEE Oceans 2009 – Europe*.

[24] A.R. Washburn (2010) 'A multistatic sonobuoy theory', report NPS-OR-10-005 of the Naval Postgraduate School, Monterey CA.

[25] S. Simakov (2008) 'Localisation in airborne multistatic sonars', *IEEE Journal of Oceanic Engineering*, vol. 33, pp. 278–88.

[26] M.P. Fewell & J.M. Thredgold (2009) 'Cumulative track-initiation probability as a basis for assessing sonar-system performance in anti-submarine warfare', technical note DSTO-TN-0932 of the Defence Science and Technology Organisation.

[27] M.P. Fewell, S. Ozols & P.K. Rzetelski (2011) 'Remote multistatic receiver field as a surveillance barrier in anti-submarine warfare', technical report DSTO-TR-2573 of the Defence Science and Technology Organisation, CLASSIFIED.

[28] S. Ozols & M.P. Fewell (2011) 'On the design of multistatic sonobuoy fields for area search', technical report DSTO-TR-2563 of the Defence Science and Technology Organisation.

[29] R.J. Urick (1983) *Principles of underwater sound*, 3rd edn, McGraw-Hill, New York.

[30] S. Simakov, Z.Y. Zhang & L. Kelly (2009) 'Australian (DSTO) modelling methodology and cross-evaluation results', report to the September 2009 meeting of the 'Advancing Multistatic Operational Capability' workshop of Technical Panel 9, Maritime Systems Group, The Technical Cooperation Program.

[31] B.C. Travaglione & T. Forward (2007) 'Transmitter–receiver separation for multistatic sonar', technical note DSTO-TN-0735 of the Defence Science and Technology Organisation.

[32] N.J. Willis (2005) *Bistatic radar* (2nd edn, corrected printing), Raleigh NC, SciTech Publishing.

[33] J.D. Lawrence (1972) *A catalogue of special plane curves*, Dover, New York.

[34] S. Ozols, M.P. Fewell & J.M. Thredgold (2011) 'Track-initiation probability for multistatic sonar fields', technical note DSTO-TN-1021 of the Defence Science and Technology Organisation.

[35] P.H. Dahl, J.H. Miller, D.H. Cato & R.K. Andrew (2007) 'Underwater ambient noise', *Acoustics Today*, vol. 3, pp. 23–33.

[36] R.B. Lindsay and R.T. Beyer (1989) 'Acoustics' in H.L. Anderson (ed.) *A physicists' desk reference*, 2nd edn, American Institute of Physics, New York.

[37] C.G. Hempel (2007) 'Track initialisation for multistatic active sonar systems', *Proceedings IEEE Oceans 2007 – Europe*.

[38] C.G. Hempel & J. Pacheco (2009) 'Performance analysis of the probabilistic multi-hypothesis tracking algorithm on the SEABAR data sets', *Proceedings 12th International Conference on Information Fusion*, Seattle.

[39] O. Gerard, S. Coraluppi, C. Carthel & D. Grimmett (2006) 'Benchmark analysis of NURC multistatic tracking capability', *Proceedings 9th International Conference on Information Fusion*, Florence.

[40] D.W. Krout, M.A. El-Sharkawi, W.J.L. Fox & M.U. Hazen (2006) 'Intelligent ping sequencing for multistatic sonar systems', *Proceedings 9th International Conference on Information Fusion*, Florence, pp. 237–42.

[41] D.W. Krout, W.J.L. Fox & M.A. El-Sharkawi (2009) 'Probability of target presence for multistatic sonar ping sequencing', *IEEE Journal of Oceanic Engineering*, vol. 34, pp. 603–9.

[42] A. de Roos, J.J. Sinton, P.T. Gough, W.K. Kennedy & M.J. Cusdin (1988) 'The detection and classification of objects lying on the seafloor', *Journal of the Acoustical Society of America*, vol. 88, pp. 1456–77.

[43] B. Gillespie, K. Rolt, G. Edelson, R. Shaffer & P. Hursky (1998) 'Littoral target forward scattering', in S. Lees & L.A. Ferrari (eds) *Acoustical Imaging 23*, New York, Plenum Press, pp. 501–6.

[44] T.C. Yang (2007) 'Acoustic dopplergram for intruder defence', *Proceedings IEEE Oceans 2007*.

[45] M. Abramowitz & I. Stegun (1868) *Handbook of Mathematical Functions*, Dover Publications, New York, 5th printing.

[46] W.H. Beyer (ed.) (1973) *CRC standard mathematicval tables*, 25th edn, CRC Press, Boca Raton FL.

[47] C.M. Traweek & T.A. Wettergren (2006) 'Efficient sensor characteristic selection for cost-effective distributed sensor networks', *IEEE Journal of Oceanic Engineering*, vol. 31, pp. 480–6.

[48] C.G. Hempel (2006) 'Adaptive track detection for multistatic active sonar', *Proceedings IEEE Oceans 2006*.

This page is intentionally blank

DEFENCE SCIENCE AND TECHNOLOGY ORGANISATION DOCUMENT CONTROL DATA	1. PRIVACY MARKING/CAVEAT (OF DOCUMENT)

2. TITLE	3. SECURITY CLASSIFICATION (FOR UNCLASSIFIED REPORTS THAT ARE LIMITED RELEASE USE (L) NEXT TO DOCUMENT CLASSIFICATION)
Simple Detection-Performance Analysis of Multistatic Sonar for Anti-Submarine Warfare	Document (U) Title (U) Abstract (U)
4. AUTHOR(S)	5. CORPORATE AUTHOR
M.P. Fewell and S. Ozols	DSTO Defence Science and Technology Organisation PO Box 1500 Edinburgh South Australia 5111 Australia

6a. DSTO NUMBER	6b. AR NUMBER	6c. TYPE OF REPORT	7. DOCUMENT DATE
DSTO-TR-2562	AR-015-022	Technical Report	June 2011

8. FILE NUMBER	9. TASK NUMBER	10. TASK SPONSOR	11. NO. OF PAGES	12. NO. OF REFERENCES
2010/1016263/1	NAV 07/338	COMFLOT	49	48

DSTO Publications Repository	14. RELEASE AUTHORITY
http://dspace.dsto.defence.gov.au/dspace/	Chief, Maritime Operations Division

15. SECONDARY RELEASE STATEMENT OF THIS DOCUMENT

Approved for public release

OVERSEAS ENQUIRIES OUTSIDE STATED LIMITATIONS SHOULD BE REFERRED THROUGH DOCUMENT EXCHANGE, PO BOX 1500, EDINBURGH, SA 5111

16. DELIBERATE ANNOUNCEMENT

No Limitations

17. CITATION IN OTHER DOCUMENTS Yes

18. DSTO RESEARCH LIBRARY THESAURUS

Sonar performance, Multistatics, Sonobuoys, Sonar detection, Track-initiation probability

19. ABSTRACT

This report describes a method of deriving the detection performance of a multistatic sonar field from the performance of a field of similar sonars operated monostatically. It allows a direct comparison of the two modes of operation, thereby quantifying the advantage, if any, of multistatics. The method is derived from the sonar equation in the noise-limited regime. We also compare two different network architectures for tracking: each receiver performing its own tracking or detection information being passed to a central tracking node. We start with three schematic monostatic detection-probability curves, ranging from almost a cookie cutter to an exponential shape, which has a long low-probability tail. We find that networking, whether to perform multistatics or to centralise tracking, brings no advantage for a cookie-cutter detection probability. With the exponential shape, on the other hand, a multistatic field can be spaced at about twice the separation for the same detection performance as a field of similar sonars operated monostatically. That is, a given area can be covered with about one quarter the number of sensors. Centralising the tracking allows about an additional third increase in sonar separation.